Research Square

Preprints are preliminary reports that have not undergone peer review.
They should not be considered conclusive, used to inform clinical practice,
or referenced by the media as validated information.

An adipocyte-endothelial framework to identify molecular signatures of metabolic vulnerability in obesity

Vaishali Chaurasiya
Minerva Foundation Institute for Medical Research, and Doctoral Programme in Clinical Research, University of Helsinki – Helsinki, Finland

Luyang Li
Division of Infection and Immunity, School of Medicine, and Systems Immunity Research Institute, Cardiff University – Cardiff, United Kingdom

Aina Lluch
Girona Biomedical Research Institute (IDIBGI), and CIBER de la Fisiología de la Obesidad y la Nutrición (CIBEROBN) – Girona, Spain

Ana Fernández-Sánchez
Girona Biomedical Research Institute (IDIBGI) – Girona, Spain

Jukka Harju
Department of Gastrointestinal Surgery, Abdominal Center, University of Helsinki and Helsinki University Hospital – Helsinki, Finland

Dan Duc Pham
Minerva Foundation Institute for Medical Research – Helsinki, Finland

Sanni Perttunen
Minerva Foundation Institute for Medical Research – Helsinki, Finland

Salla Keskitalo
Molecular Systems Biology Research Group & Proteomics Unit, HiLIFE Helsinki Institute of Life Science, Institute of Biotechnology, University of Helsinki – Helsinki, Finland

Markku Varjosalo
Molecular Systems Biology Research Group & Proteomics Unit, HiLIFE Helsinki Institute of Life Science, Institute of Biotechnology, University of Helsinki – Helsinki, Finland https://orcid.org/0000-0002-1340-9732

Kirsi H. Pietiläinen
Obesity Research Unit, Research Program for Clinical and Molecular Metabolism, and HealthyWeightHub, Endocrinology, Abdominal Center, Helsinki University Hospital, University of Helsinki – Helsinki, Finland

P.A. Nidhina Haridas
Minerva Foundation Institute for Medical Research – Helsinki, Finland

José-Maria Moreno-Navarrete
Girona Biomedical Research Institute (IDIBGI), CIBER de la Fisiología de la Obesidad y la Nutrición (CIBEROBN), and School of Medicine, University of Girona – Girona, Spain
José I. Rodríguez-Hermosa
Girona Biomedical Research Institute (IDIBGI), and School of Medicine, University of Girona – Girona, Spain
Encarna Piedrafita-Serra
Girona Biomedical Research Institute (IDIBGI), and School of Medicine, University of Girona – Girona, Spain
Asha Kar
Bioinformatics Interdepartmental Program, and Institute for Precision Health, David Geffen School of Medicine, UCLA – Los Angeles, USA
Päivi Pajukanta
Bioinformatics Interdepartmental Program, and Institute for Precision Health, David Geffen School of Medicine at UCLA – Los Angeles, USA
Markku Laakso
Institute of Clinical Medicine, University of Eastern Finland and Kuopio University Hospital – Kuopio, Finland
Ville Männistö
Institute of Clinical Medicine, University of Eastern Finland and Kuopio University Hospital – Kuopio, Finland
Jussi Pihlajamäki
Institute of Public Health and Clinical Nutrition, University of Eastern Finland and Kuopio University Hospital – Kuopio, Finland
Minna U. Kaikkonen
A.I. Virtanen Institute for Molecular Sciences, University of Eastern Finland – Kuopio, Finland
Gema Frühbeck
Instituto de Investigación Sanitaria de Navarra (IdISNA), Clínica Universidad de Navarra, and CIBER de la Fisiología de la Obesidad y la Nutrición – Pamplona, Spain https://orcid.org/0000-0002-8305-7154
Oriol A. Rangel-Zúñiga
Maimónides Biomedical Research Institute of Córdoba (IMIBIC), Reina Sofia University Hospital, University of Córdoba, and CIBER de la Fisiología de la Obesidad y la Nutrición – Córdoba, Spain
Francisco José Tinahones
Instituto de Investigación Biomédica de Málaga (IBIMA), Virgen de la Victoria Hospital, University of Málaga, and CIBER de la Fisiología de la Obesidad y la Nutrición – Málaga, Spain
Carlos Dieguez
Center for Research in Molecular Medicine and Chronic Diseases (CiMUS, University of Santiago de Compostela, Instituto de Investigación Sanitaria, CIBER de la Fisiología de la Obesidad y la Nutrición – Santiago de Compostela, Spain
Ralph Burkhardt

Institute of Clinical Chemistry and Laboratory Medicine, University Hospital Regensburg – Regensburg, Germany

Marcus Höring
Institute of Clinical Chemistry and Laboratory Medicine, University Hospital Regensburg – Regensburg, Germany

Gerhard Liebisch
Institute of Clinical Chemistry and Laboratory Medicine, University Hospital Regensburg – Regensburg, Germany

Johanna Pörschke
Institute for Tumor Immunology, Center for Tumor Biology and Immunology, Marburg University – Marburg, Germany

María Gómez-Serrano
Institute for Tumor Immunology, Center for Tumor Biology and Immunology, Marburg University – Marburg, Germany

Johannes Graumann
Institute of Translational Proteomics & Core Facility, Marburg University – Marburg, Germany

Witold Szymanski
Institute of Translational Proteomics & Core Facility, Marburg University – Marburg, Germany

José-Manuel Fernández-Real
Girona Biomedical Research Institute (IDIBGI), CIBER de la Fisiología de la Obesidad y la Nutrición (CIBEROBN), and School of Medicine, University of Girona – Girona, Spain

You Zhou
Division of Infection and Immunity, School of Medicine, and Systems Immunity Research Institute, Cardiff University – Cardiff, United Kingdom

Vesa Olkkonen
vesa.olkkonen@helsinki.fi

Minerva Foundation Institute for Medical Research, and Department of Anatomy, Faculty of Medicine, University of Helsinki – Helsinki, Finland

Francisco Ortega
fortega@idibgi.org

Girona Biomedical Research Institute (IDIBGI), and CIBER de la Fisiología de la Obesidad y la Nutrición (CIBEROBN) – Girona, Spain

---

Article

Keywords: Adipose tissue, adipocyte, endothelial cell, proteomics, lipidomics, meta-inflammation, obesity, weight loss

Posted Date: April 23rd, 2026

DOI: https://doi.org/10.21203/rs.3.rs-9485802/v1

License: This work is licensed under a Creative Commons Attribution 4.0 International License.
Read Full License

Additional Declarations: There is no conflict of interest

Abstract

Obesity-related metabolic disease is linked to impaired adipose tissue function, but the underlying molecular programs are difficult to assign to specific adipose-resident cell types, to mechanistically connect to inflammation, and to distinguish from alterations that normalize with weight loss. We integrated here a layered design combining untargeted proteomics and lipidomics to define obesity-associated, cell-type-resolved molecular phenotypes across isolated adipocytes and adipose microvascular endothelial cells, explore whether an obesity-like inflammatory milieu reproduces adipose-resident cell dysfunction, and identify molecular features that show evidence of recovery after surgery-induced weight loss. As expected, adipocytes from people with obesity show suppression of mitochondrial energy metabolism together with impaired lipid plasticity, as reflected by triglyceride remodelling. By mimicking an obesity-like inflammatory milieu with macrophage-conditioned media, we reproduced most of these changes in adipocyte cultures. Endothelial cells exhibited yet another, opposite trajectory in obesity, with reduced cell-cycle signalling and increased mitochondrial activation, which were recapitulated in vitro when these cells were exposed, respectively, to the secretions of inflamed macrophages and adipocytes. Bulk adipose tissue proteomes and lipidomes showed evidence of metabolic improvement after weight loss, with broad restoration of mitochondrial and substrate-handling pathways and reciprocal triglyceride remodelling. Alongside the inflammation-responsive adipocyte mitochondrial and lipid-handling dysfunction, our cell-type-informed framework probes macrophage and adipocyte-to-endothelial activation in obesity and delineates cross-context cellular programs that recover with weight loss. Additionally, we identified the elements that exhibit the strongest association with dyslipidaemia, hypertriglyceridemia and hyperglycaemia in individuals with obesity, confirming molecular signatures relevant to metabolic obesity in two cross-sectional samples.

Vaishali Chaurasiya, Luyang Li, Aina Lluch participated equally

INTRODUCTION

Obesity is increasingly common worldwide [1] and strikingly associated with an elevated risk of metabolic and cardiovascular disease [2]. A central link between excessive adiposity and cardiometabolic complications is impaired adipose tissue function, mainly characterized by chronic low-grade inflammation interfering with mitochondrial metabolism, lipid storage, endocrine signalling, and tissue homeostasis [3–5]. Importantly, many pathological consequences attributed to obesity are thought to reflect not adipose mass per se, but altered cellular programs within fat depots (particularly in adipocytes and the stromal vascular niche) that can impair adipose synthetic, oxidative, and secretory functions [6,7]. Indeed, adipose tissue is an essential, complex, and highly dynamic metabolic organ whose capacity to expand, contract, and regulate systemic energy balance is fundamental in both health and disease [8]. Even in the context of the debated concept of “metabolically healthy” obesity [9,10], adipocyte

metabolism and endocrine activity can become disrupted, paralleling changes in adipose-resident macrophage activation [11,12], progenitor cell commitment [13], and endothelial cell (EC) biology [14,15].

Adipose tissue is highly vascularized [16,17], and its vasculature is not merely a passive supply network. Beyond oxygenation and nutrient/waste transport, blood vessels shape exposure to circulating hormones and growth factors, enable trafficking of immune and stromal cells, and influence fatty acid mobilization, processes integral to adipose metabolic and endocrine function [18]. Adipose-resident EC themselves participate in lipid handling, energy homeostasis, and metabolic health [19]. Over the last decade, impaired vascular density and EC dysfunction have emerged as hallmarks of excessive adiposity [20]. Vascular adaptation is also tightly coupled to adipose remodelling: adipose expansion depends on angiogenesis [21,22], while the adipose microenvironment (e.g., hypoxia, inflammatory cues, and paracrine signals from adipose cells) can either promote or blunt EC responses [14,23,24]. Because the mural cell compartment of adipose vasculature contains progenitor cells that can differentiate into adipocytes [25], the immune-vascular-adipocyte axis is positioned to influence both depot remodelling and metabolic risk.

Despite already available extensive transcriptomic profiling of adipose tissue in obesity, two shortcomings limit physiological interpretation. First, bulk tissue signatures conflate changes in cell-intrinsic programs with shifts in cellular composition, making it difficult to assign key pathways to specific adipose cell types. Second, it remains unclear which obesity-associated molecular alterations represent reversible dysfunction (i.e., programs that recover with weight loss) as opposed to context-specific correlation. Addressing these gaps requires integration across cell types, perturbation models that mimic the inflammatory adipose milieu, and within-person evidence of recovery following clinically meaningful weight loss. Here, we combined flow cytometry-based cell isolation with untargeted, omics-scale proteomic and lipidomic profiling to resolve adipocyte and EC-specific molecular phenotypes across complementary contexts relevant to obesity pathophysiology. We profiled ex vivo isolated adipocytes and adipose-resident EC from individuals in the lean body weigh range and individuals living with obesity, modelled obesity-like inflammatory stress in vitro using macrophage-conditioned media (MCM) and adipocyte-conditioned media (ACM) to address adipocyte-to-EC signalling, and assessed recovery-associated remodelling in paired bulk adipose tissue before and after bariatric surgery-induced weight loss. We further integrated these layers of information with several independent transcriptomic resources and cohort data to prioritize robust adipocyte and EC determinants linked to impaired metabolism. Together, our framework identifies non-immune adipose cell-type-informed molecular determinants altered in obesity, reveals which are inflammation-responsive, and delineates adipocyte and EC-linked programs that show evidence of recovery with weight loss, providing molecular signatures of metabolic vulnerability in people with obesity.

METHODS

Cohorts. For the study of *ex vivo* isolated adipocytes and adipose-resident EC (cohort #1), ~5 g of omental adipose tissue were retrieved from 17 patients (2 men and 15 women) undergoing surgical cholecystectomy for gallstone disease at the Department of Gastrointestinal Surgery, Abdominal Center, HUS Jorvi hospital of Helsinki, in Finland (**Table S1**). Upon extraction, adipose samples were transferred to the laboratory and processed under sterile conditions within 24 hours, as further explained in reference [26]. In the longitudinal study (cohort #2), abdominal subcutaneous adipose tissue was collected in eighteen (n=18) surgical patients with severe obesity (2 men and 16 women) during and after enduring laparoscopic Roux-en-Y gastric bypass and subsequent weight loss (**Table S2**). Macrobiopsies of adipose tissue were minced in pieces of ~150 mg immediately after extraction, then introduced in sterile containers, snap frozen in liquid nitrogen, and stored at minus 80ºC until further processing. Human samples were handled following standard operating procedures, and information from subjects included in this study was provided by the FATBANK platform, promoted by the CIBEROBN and coordinated by the Biomedical Research Institute of Girona (IDIBGI) Biobank (Biobank IDIBGI), integrated in the Spanish National Biobanks Network (ISCIII, Madrid). All subjects provided written informed consent before entering the study, which was approved by the Ethics Committees for Clinical Investigation (CEIC) of the Biobanc IDIBGI (ethics approval study number B.0000872) and the Helsinki and Uusimaa Hospital District (ethics approval study number HUS/23/2022), respectively. For validation purposes, we reanalysed bulk adipose RNA-seq data available in three independent samples. The METabolic Syndrome In Men (METSIM; ethics approval study number 171/2004) sample (cohort #3) consists of 10,197 Finnish males with ages between 45 and 73, recruited in the University of Eastern Finland and Kuopio University Hospital, Kuopio, Finland, as described in detail in reference [27]. The study design was approved by the Ethics Committee of the Northern Savo Hospital District, and all participants gave written informed consent. All research conformed to the principles of the Helsinki Declaration, and bulk RNA-seq data was obtained in the subcutaneous adipose tissue of 335 unrelated participants [27,28] (**Table S3**). The cohort #4 (Finnish Twin Cohort) consisted of 49 twin pairs discordant for clinical characteristics of obesity [29] (ethics approval study number 270/13/03/01/2008). The cohort #5 involved 451 obese adults (30.6% men) from the ADIPOMIT cohort [30] (**Table S4**), including patients who had undergone surgical intervention between 2009 and 2020, and allowed the removal of fat for biomedical research, given written informed consent. The replication analysis in cohort #6 was selected for confirmatory purposes in the bulk RNA-seq of 259 obese adults (30.7% men) from the Kuopio OBesity Surgery (KOBS) cohort [4] (**Table S5**). The ADIPOMIT study (ethics approval study number 2019.062) was approved by the Ethics Committee of the Hospital Dr Josep Trueta of Girona (Spain). The KOBS workflow (ethics approval study numbers 54/2005, 104/2008, and 27/2010) was approved by the Ethics Committee of the Northern Savo Hospital District (Finland).

Clinical measures. Weight and height were measured after a 12-hours overnight fast in light clothing. BMI was calculated as weight (in kilograms) divided by height (in meters) squared. Obesity was defined when BMI≥30 kg/m^2. Blood pressure was measured in the supine position on the right arm after a 10 min rest.

A standard sphygmomanometer of appropriate cuff size was used, and the first and fifth phases were recorded. Blood samples were collected following an overnight fast. Samples were analyzed at the corresponding core facilities of participating hospitals in Girona and Helsinki, using standardized methods. Concentrations of plasma glucose were measured using the spectrophotometric hexokinase and glucose-6-phosphate dehydrogenase assay in a Beckman Glucose Analyzer 2 (Beckman Coulter). Measures of total cholesterol were obtained by enzymatic methods on a BM/Hitachi 747 analysis system (Roche), and high (HDL) and low (LDL) density lipoprotein cholesterol were quantified after precipitation with polyethylene glycol 6000 at a final concentration of 100 g/l. Blood hemoglobin (HbA1c) was measured during routine laboratory tests, and blood triglycerides were quantified by the reaction of glycerol-phosphate-oxidase and peroxidase on a Hitachi 917 Rack Chemistry Analyzer (Roche). All participants were requested to withhold alcohol and caffeine prior to the analyses.

Adipose-resident cell isolation. Adipose tissue was obtained from the intra-abdominal area of gallstone patients undergoing surgical cholecystectomy. The biopsies were immersed in cold phosphate-buffered saline (PBS) containing 2% penicillin/streptomycin and promptly transported to the laboratory on ice. Collected tissue was immediately processed for isolation of adipocytes and adipose-resident microvascular EC. Adipocytes and EC were segregated according to our standardized protocol, as described in reference [26]. Briefly, the extracellular matrix was digested in 90 rpm shaking incubator with collagenase II buffer (Gibco, Paisley, UK) for 20–25 min at 37°C. Digested fat solution was gently poured through a sterile 250 μm mesh filter (Sintab, 6111–025043), gently squeezed and further rinsed twice with PBS. The cell suspension was then transferred to a sterile separation funnel and allowed to stand for 3 min. Adipocytes were then collected and incubated for 5 min with 5 ml of 1xRBC lysis buffer (eBioscience, 00-4300-54) to remove red blood cells, further washed twice with PBS, collected to 50 ml falcon tubes from the separation funnel, and centrifuged at 50×g for 3 min. Then, three aliquots of adipocytes (150-300 μl) were snap frozen in liquid nitrogen for multi-omic study preparation. The stromal vascular cells (SVC) were centrifuged at 1,000 rpm for 5 minutes at 4°C, after which the pellet was incubated with 1× RBC lysis buffer and subsequently washed with PBS. The resulting SVC pellet was resuspended in culture medium and transferred to a T-75 culture flask. SVC were cultured and maintained in a 5% CO_2 incubator at 37°C in a humidified atmosphere, with endothelial cell growth media (PromoCell, C-22011). Then, EC were isolated using fluorescence-activated cell sorting (FACS) with antibodies against positive CD31 and CD144 in CD45 negative SVC, subsequently cultured in ECGM media, and passaged twice before preparing proteomics samples.

Cell cultures. Commercially available cryopreservedpreadipocytes obtained in one Caucasian women aged 30-50 years and BMI of 25-30 kg/m^2 (SP-F-2) were purchased (Zen-Bio, Inc.). To induce the adipogenic conversion, adipocyte progenitors were led to grow in preadipocyte medium (PM-1), then incubated with adipocyte differentiation medium (DM-2) for 7 days. This media is composed of DMEM/Ham's F-12 (1:1), HEPES, FBS, biotin, pantothenate, insulin, dexamethasone, IBMX, PPARγ agonist, penicillin, streptomycin and amphotericin B. Thereafter, differentiating adipocytes were maintained in adipocyte maintenance (AM-1) media (i.e., DM-2 without IBMX and PPARγ agonists) for 7

days. The human monocyte cell line THP-1 (ATCC, TIB-202) was cultured in RPMI 1640 medium (Gibco, 21875-034) containing 10% FBS, 5 mM glucose (Sigma, G8644), 2 mM L-glutamine, 50 mg/ml Gentamicin (Gibco, 15710-064), and 20 mM HEPES. Floating monocytes were then incubated for 24 h with 0.162 mM phorbol 12-myristate 13-acetate (Merck, P1585) to induce the adherent pro-inflammatory type 1 macrophage-like state (M1). M1 macrophages were washed with PBS and incubated 24 h with fresh medium containing 10 ng/ml LPS (Sigma, L4516). The resulting macrophage LPS-conditioned medium (MCM) was collected and centrifuged at 400*g* for 5 min, filtered, diluted in adipocyte media, and applied to adipocyte cultures for 72 h. Preadipocytes were maintained in PM-1 media during the whole process, and used as reference control. Both differentiated control adipocytes treated with macrophage media and MCM-treated adipocytes were collected and used for analyses. After 72 h from the last medium change, each supernatant was collected, centrifuged for 10 min at 1500 rpm, filtered to eliminate any debris, and indicated as adipocyte MCM-conditioned medium (ACM) or control. ACM was stored at -80°C for further experiments. Human adipose microvascular endothelial cells (HAMEC) were purchased (PeloBiotech, Planegg/Martinsried, Germany) and cultured upon arrival in ECGM media with 1x supplement (PromoCell, C-22011). At passage 4, they were incubated for 72 h with either 1% control media (RPMI with 1% PS and 10% FBS) or 1% MCM, or with 10% ACM or control. Post-treatment, EC were washed twice with PBS, before being lysed using freshly prepared RIPA buffer with 1% SDS (MCM-HAMEC), or 8M urea in 50 mM ammonium bicarbonate (ACM-HAMEC).

Proteomics. Bulk human adipose tissue samples (study #3), and adipocyte, progenitor cell, and MCM-HAMEC cultures (study #2) were transferred to the Philipps-Universtität, in Marburg, Germany. Protein amounts were assessed using a Bruker timsTOF Ultra by the Core Facility Translational Proteomics. Isolated adipocytes and adipose-resident EC (study #1), and ACM-HAMEC cultures (study #2) were dispatched to the Proteomics Unit of the Institute of Biotechnology at the University of Helsinki for proteomic assessment, using liquid chromatography tandem mass spectrometry (LC-MS/MS) on a Bruker timsTOF Pro. The protocol for proteomic sample preparation in isolated adipocytes, which are characterized by extreme lipid content, was adapted from the literature [31]. To begin with, 500 µl of proteomic lysis buffer [1% (wt/vol) sodium deoxycholate in 100 mM triethylammonium] was added to flash-frozen adipocytes, which were then lysed using a tissue homogenizer. The lysates were centrifuged at 6,000*g* for 15 min at 4°C. Cleared lysate was carefully removed by a 1 ml syringe and further sonicated and heat incubated at 95°C for 5 minutes. To extract proteins from the lysate, methanol and chloroform extraction was carried out as described [26]. Specifically, protein extraction was done using methanol and chloroform in a 4:1 ratio. 800 µl of methanol was added to 200 µl of protein lysate and vortexed thoroughly, followed by the addition of 200 µl of chloroform. Subsequently, 600 µl of H_2O was added and the sample was centrifuged for 1 minute at 14,000*g*. After centrifugation, the samples were phase separated into three layers and the top aqueous layer was discarded without disturbing the interphase protein precipitate. Following this, 800 µl of methanol was added to the remaining layers, vortexed, and centrifuged for 5 minutes at 20,000*g*. The supernatant was then discarded, and the protein pellet resuspended into 200 µl of the above protein lysis buffer. In parallel, adipose-resident EC were rinsed with PBS twice, and 140 µl of 8 M urea in 50 mM ammonium

bicarbonate buffer were used for lysis. The protein concentration of adipocytes and EC samples was measured using the Pierce™ BCA Protein Assay Kit (Thermo Scientific™, 23225), according to the manufacturer's protocol. The proteomic analysis was conducted using 10 µg of adipocyte-derived proteins and 20 µg of sample from EC. Adipocyte samples were brought to 200 µl with 50 mM NH_4HCO_3 and EC samples to 150 µl. Next, 5 mM TCEP [Tris(2-carboxyethol) phosphine hydrochloride salt, #C4706 Sigma-Aldrich, USA] was incubated at 37 °C for 30 min to reduce the samples. For alkylation, 10 mM iodoacetamide (Acros Organics, 122271000) was used for 30 minutes at room temperature, and samples were trypsin digested using 1:20 enzyme to protein ratio Sequencing Grade Modified Trypsin (Promega, V5113) for 16 h at 37°C. Further, 10% trifluoroacetic acid (TFA, VWR, 85049.051) was used to acidify the samples. The AC samples were then centrifuged 16,000 xg, 10 min at room temperature to precipitate the sodium deoxycholate in the buffer, and desalting was done for both sample types using BioPureSPN PROTO 300 C18 Mini columns (HUM S18V, Nest Group) according to the manufacturer's protocol. Thereafter, a centrifuge concentrator (Concentrator Plus, Eppendorf) was used to dry the peptide samples, which were reconstituted in 30 µl buffer A [0.1% TFA, 1% acetonitrile (VWR) in HPLC grade water (Fisher)]. The samples were diluted 1:20 in 0.1 % formic acid in HPLC water and loaded into Evotip Pure (Evosep, EV2011) according to the manufacturer's protocol. An Evosep One (Evosep) Chromatography system coupled to a hybrid trapped ion mobility quadrupole TOF mass spectrometer with a CaptiveSpray nano-electrospray ion source (Bruker Daltonics) was used to analyze the samples. Mobile phase A (0.1 % formic acid in water) and mobile phase B (0.1 % formic acid in acetonitrile) were used for phase separation in conjunction to an 8 cm × 150 µm column [1.5 µm C18 beads (Evosep, EV1109)]. MS analysis was done using positive-ion mode and MSFragger pipeline (FragPipe analysis platform (version 20.0) with MSFragger (version 3.8)[32], Philosopher (version 5.0.0), and IonQuant (version 1.9.8) for peptide identification using raw (.d) files as input). Uniprot reference human proteome UP000005640 was used as protein sequence database (see in supplemental **Table S6**). For studies #2 and #3, protein lysates were obtained as previously described by Gómez-Serrano *et al*. [33]. Briefly, 80-100 mg of adipose tissue were homogenized in 150 µl of RIPA buffer (Thermo, 89901) supplemented with 1:100 Halt Protease and Phosphatase Inhibitor Cocktail (Thermo, 78442) by using the Sample Grinding Kit (Cytiva, 80-6483-37). Manufacturer's instructions were slightly adapted to the lipid nature of human fat, including two grinding-centrifugation steps using 2/3 and 1/3 of the lysis volume, respectively. All steps were done at 4°C, including a final additional clean-up centrifugation step of collected protein supernatants. Protein concentration was estimated by Pierce™ BCA Protein Assay Kit (Thermo, 23225). Next, protein extracts were prepared for MS-based proteomics using a modified single-pot, solid-phase-enhanced sample preparation (SP3) method [34]. This protocol integrates protein extraction and detergent removal with C18 solid phase extraction (SPE) for peptide desalting, according to an in-house protocol (http://doi.org/10.5281/zenodo.17570946), with minor modifications. 50 µg of protein per sample was used for preparation. The SP3 procedure was performed in 500 µL Eppendorf Tubes. Chromabond C18WP spin columns were utilized for the C18 SPE desalting step. The final peptide concentration was equalized to 25 ng/µL for injection onto the analytical column. Peptide injection, separation and measurement on Bruker timsTOF Ultra as well as subsequent spectrum matching with Dia-NN was

performed as described in http://doi.org/10.5281/zenodo.17475274. For study #3 (bulk adipose tissue), sample loading was performed in “oneCol” mode, loading directly onto the analytical column and omitting the trap-column. MS acquisition was operating in “sensitive” mode. For study #3 (adipocytes), sample loading was equally performed in “oneCol” mode, and the gradient extended to 90 min. For HAMEC, the gradient length was shortened to 45 min. Spectrum matching was performed against the Human Uniprot.org database. All databases used are uploaded along with the description to the repository (see below the **Data availability** section). Downstream data processing and statistical analysis used the Autonomics package developed in-house (Bioconductor: 10.18129/B9.bioc.autonomics, version: 1.17.16, 1.1.7.14, 1.15.145, 1.15.235, or 1.15.345). Proteomic data were filtered to retain proteins with summed MaxLFQ intensity greater than zero across replicates in both the study and control groups. MaxLFQ intensities were subsequently log2 transformed. Raw log2 intensities (Study #1 and #3) or MaxLFQ intensities (Study #2) were used for quantitation. Measurements from only two precursors (Np) per sample were converted to NA (Not Applicable) for that particular sample. Proteins with a q-value of <0.01 were included for further analysis. Differential abundance of protein groups was evaluated using the Limma package (version 3.54.2) [35]. The R version 4.2.3 (https://www.r-project.org/) code used for processing of spectrum matching (FragPipe and Dia-NN) output data and statistical analysis has been uploaded along with the mass spectrometric raw data to the ProteomeXchange Consortium (see below the **Data availability** section). Finally, the org.Hs.eg.db (version 3.16.0) package (https://www.bioconductor.org) was used to map gene symbols to their corresponding Entrez gene IDs. Reference gene sets for pathway enrichment analysis were obtained from the Gene Ontology (https://geneontology.org), the Kyoto Encyclopedia of Genes and Genomes (KEGG) (https://www.genome.jp/kegg/), and the Molecular Signatures Database (https://www.gsea-msigdb.org/gsea/msigdb). Differentially expressed proteins were analyzed for over-representation analysis (ORA) using the “enrichGO”, “enrichKEGG”, and “enrichr” functions from the clusterProfiler package (version 4.6.2) [36] to identify enriched GO, KEGG, and Hallmark pathways, respectively. For Gene Set Enrichment Analysis (GSEA), a ranking metric was computed by multiplying the negative logarithm of the p-value by the sign of the log2FC for all proteins, and then sorting the results in descending order. Ranked gene lists were transformed into a named vector format for downstream GSEA implementation with the “gseGO”, “gseKEGG”, and “GSEA” functions. The enriched pathways were visualized using the ggplot2 (version 3.4.4) package. All these pathway analyses were performed in the R environment.

Lipidomics. Bulk adipose tissue, *in vitro* cultures of adipocyte and precursor cells, and *ex vivo* isolated adipocytes for lipidomics were handled in the Lipidomics Lab Regensburg, located at the Institute of Clinical Chemistry and Laboratory Medicine of the University Hospital of Regensburg (Germany). Lipid composition was measured by mass spectrometry (MS) for direct flow injection analysis, coupled to liquid (LC) and gas chromatography (GC). An amount of 2 mg wet weight (adipose tissue), 1-10 µg protein (isolated mature adipocytes), or about 100 µg protein (primary human adipocytes) were subjected to lipid extraction according to the protocol by Bligh and Dyer [37], with internal standards added to each sample prior to lipid extraction. For flow injection analysis, the lipid extract was vacuum-dried and afterwards dissolved in chloroform/methanol/2-propanol (1:2:4 v/v/v) with 7.5 mM ammonium or in

chloroform/methanol (1:1 v/v/v) with 7.5 mM ammonium formate (for measurement of triglycerides). For hydrophilic interaction liquid chromatography (HILIC)-MS/MS, the lipid extract was injected in chloroform. The analysis of lipids was performed by direct flow injection analysis (FIA) using a triple quadrupole mass spectrometer (FIA-MS/MS) and a high-resolution hybrid quadrupole-Orbitrap mass spectrometer (FIA-FTMS). FIA-MS/MS was performed in positive ion mode using the analytical setup and strategy described previously [38]. A fragment ion of *m/z* 184 was used for lysophosphatidylcholines (LPC) [39]. The following neutral losses were applied: Phosphatidylethanolamine (PE) and lysophosphatidylethanolamine (LPE) 141, phosphatidylserine (PS) 185, phosphatidylglycerol (PG) 189 and phosphatidylinositol (PI) 277 [40]. Sphingosine based ceramides (Cer) and hexosylceramides (Hex-Cer) were analyzed using a fragment ion of *m/z* 264 [41]. PE-based plasmalogens (PE P) were analyzed according to the principles described by Zemski-Berry [42]. Cardiolipin was monitored by diglycerol fragment ions [43]. Glycerophospholipid species annotation was based on the assumption of even numbered carbon chains only. Detailed description of the FIA-FTMS method is available in [44]. Triglycerides (TG), diglycerides (DG) and cholesterol esters (CE) were recorded in positive ion mode *m/z* 500-1000 as $[M+NH_4]^+$ at a target resolution of 140,000 (at 200 *m/z*). CE species were corrected for their species-specific response [45]. Phosphatidylcholines (PC), PC ether (PC O) and sphingomyelins (SM) were analyzed in negative ion mode *m/z* 520-960 as $[M+HCOO]^-$ at the same resolution setting. Analysis of free cholesterol (FC) was performed after derivatization with acetyl chloride followed by multiplexed acquisition (MSX) of the $[M+NH_4]^+$ of FC (converted to cholesteryl acetate) and the deuterated internal standard (FC[D7]) [45,46]. With regard to HILIC-MS/MS, lipid extracts were subjected to HILIC coupled to MS/MS using a similar setup as described in [43]. A fragment ion of *m/z* 184 was used to quantify PC and SM [38]. Absolute intensities obtained for each lipid and sample were used for analysis. Missing values in the dataset were initially replaced with zeros and subsequently imputed by calculating half of the minimum non-zero value and introducing random noise, as described previously [47]. Relative concentrations were normalized based on the total amount within each lipid class, followed by $\log_2$ transformation for conducting Student's t-test between the study and the control group. Differential abundance of lipids was identified based on an absolute $\log_2$ fold-change (FC) value ≥ 0.58 and p-value ≤ 0.05. Quality control analyses were performed in all three substudies, and the resulting plots were visualized using the ggplot2 package (version 3.4.4). Additionally, hierarchical clustering heatmaps based on Euclidean distance were generated utilizing the pheatmap package (version 1.0.12) (https://www.bioconductor.org).

Mitochondrial function. For the mitochondrial function test, we used an Agilent Seahorse XF Pro Analyzer. SGBS-derived adipocytes were seeded into XF Pro M cell culture plates (Agilent), differentiated, and subsequently treated with 1% MCM for 72 h. HAMECs were similarly seeded and treated for 72 h with MCM or ACM, with the respective controls. Prior to run, cells were washed and incubated for 1 h in XF base medium (#103575) supplemented with 10 mM glucose (#103577), 1 mM sodium pyruvate (#103578), and 2 mM L-glutamine (G7513, Agilent) in a CO_2-free incubator. During the Seahorse XF Mito

Stress Test, Oxygen Consumption Rates (OCR) were monitored at each of the following phases: baseline, and following sequential addition of oligomycin (final concentration 10 μM), carbonyl cyanide-p-trifluoromethoxyphenyl-hydrazone (FCCP; final concentration 20 μM), and a mixture of rotenone/antimycin A (final concentration 10 μM each). Data were acquired and analyzed using Wave software (Agilent). The cell number in each well was determined using 3.3 μM Hoechst (# 62249, Thermo) staining together with a Cytation 5 Cell Imaging Multi-Mode Reader (BioTek), and used to normalize flux rates.

Mitochondrial DNA. HAMEC were treated for 72 hours with ACM and MCM, alongside their respective controls (n=3/group). DNA was isolated from cell lysates following manufacturer's instructions (#51304, Qiagen). Mitochondrial DNA (mtDNA) content was assessed by means of a LightCycler 480 II Real-Time PCR System (Roche). Expression of 16S rRNA, Cytochrome b (CYTB), and mitochondrial displacement loop (D-loop) was used as surrogates of mtDNA, while expression of Amyloid Beta Precursor Protein (APP), Beta-2-Microglobulin (B2M), and Ribosomal protein lateral stalk subunit P0 (RPLP0) was used to address genomic DNA (gDNA) content. For each target, $2^{(-\Delta CT)}$ values were calculated, and mtDNA measurements were subsequently normalized taking gDNA values as reference. Forward (Fw) and reverse (Rv) primer sequences are provided below.

16S rRNA: Fw, GGGGCGACCTCGGAGCAGAA; Rv, ATAGCGGCTGCACCATCGGGA

CYTB: Fw, GCCTGCCTGATCCTCCAAAT; Rv, AAGGTAGCGGATGATTCAGCC

D-loop: Fw, CATCTGGTTCCTACTTCAGGG; Rv, CCGTGAGTGGTTAATAGGGTG

APP: Fw, GTGTGCTCTCCCAGGTCTA; Rv, CAGTTCTGGATGGTCACTGG

B2M: Fw, TGCTGTCTCCATGTTTGATGTATCT; Rv, TCTCTGCTCCCCACCTCTAAGT

RPLP0: Fw, TGGTCATCCAGGTGTTCGA; Rv, ACAGACACTGGCAACATTGCGG

Angiogenesis assay. Following 72 hours of treatment with 10% ACM, 1% MCM, and respective control on HAMEC cultures, angiogenesis assays were conducted using the ECMatrix™ system (ECM625, Millipore). To do so, cells were seeded onto the matrix in 96-well plates according to the manufacturer's protocol (n=4/group). Tube formation was imaged at 2, 4, 6, and 8 hours using an Invitrogen EVOS™ M5000 microscope at 4× magnification. Quantification of angiogenesis was performed on binary images with the Fiji Angiogenesis Analyzer plugin1 (ImageJ) [48], measuring percentage of total segment length and total branching length.

Data analysis. To screen out differentially expressed genes (DEG), the series matrix files were downloaded and analyzed by NetworkAnalyst 3.0 (http://www.networkanalyst.ca) through Log_2 transformation normalization. Utilizing Limma, a Log_2 (fold change)>1, and p-value<0.05 were applied as the cutoff criteria. Cluster analysis and integrated bioinformatics analysis were used to visualize the interaction relationships of the DEGs in each dataset. Representative images, including heatmap, the

gene cluster in the PCA loading score, and the chord diagram of the datasets, were visualized using NetworkAnalyst 3.0. The KEGG topology enrichment analysis, protein-protein Internet (PPI) topology analysis, and Gene Regulatory Networks TF-gene interactions analyses were also applied. KEGG [49] and GO [50] analyses were performed using overrepresentation analysis methods in the Web-based Gene Set Analysis Toolkit (WebGestalt, http://www.webgestalt.org) and Metascape (http://www.metascape.org). The KEGG topology enrichment and PPI topology analyses were also performed using NetworkAnalyst 3.0. Differentially expressed proteins associated with common GO pathways were analyzed to generate alluvial diagrams. GeneRatio values were first converted into a numerical format by computing the ratio of enriched gene counts and background genes. GO pathways were then ranked based on adjusted p-values and GeneRatio values. To construct the alluvial diagram, candidate proteins were first transformed into a long format suitable for visualization. The alluvial diagram was generated using the "geom_sankey" function from the ggsankey package and visualized with ggplot2 (https://www.bioconductor.org), illustrating the flow relationships between proteins and pathways. Additionally, a dot plot was created to display GeneRatio and corresponding pathways with significant adjusted p-values. The final visualization integrates the alluvial diagram with the dot plot, aligning them through coordinate transformations and custom annotations for improved clarity. Statistical analyses were carried out with Mann-Whitney test as stated in figure captions, by using Graphpad Prism 9. In the ADIPOMIT cohort, metabolically "unhealthy" obesity (UO) was defined based on the International Diabetes Federation criteria [51], with the presence of at least one of the following traits: (a) hypertriglyceridemia (HTG), defined as triglyceride [TG]≥1.7 mmol/L (150 mg/dL); (b) dyslipidemia (DL), defined as high-density lipoprotein cholesterol [HDL] less than 1.03 mmol/L (40 mg/dL) in men, and less than 1.29 mmol/L (50 mg/dL) in women; and (c) hyperglycemia (HG), when fasting plasma glucose≥5.6 mmol/L (100 mg/dL). Participants with one or more of these metabolic alterations were categorized into the UO group, while participants with none of the above-mentioned abnormalities were categorized into the "healthy" obesity (HO) group [52]. For this study, raised blood pressures, and the presence of central obesity, defined as waist circumference [WC]≥94 cm for men, and ≥80 cm for women, were neglected, as hypertension and central obesity is assumed when BMI>30 kg/m^2. For conducting Stepwise Regression Analysis, normalized Log_2-transformed gene expression data and clinical covariates (i.e., age, sex, and BMI) were used. The outcome variable was group classification (UO vs HO), while predictors consisted of gene expression values together with covariates. Stepwise regression was performed in R using the stepAIC function from the MASS package (v7.3) (https://www.stats.ox.ac.uk/pub/MASS4/), starting from the full model and applying bidirectional selection based on the Akaike Information Criterion (AIC). The performance of the final logistic regression model was evaluated using receiver operating characteristic (ROC) curve analysis with the pROC package (v1.19) [53]. Finally, variable importance scores were calculated using multiple machine learning approaches implemented in R to assess the relative contribution of each predictor. Models included logistic regression from the caret package (v7.0) [54], random forest from the randomForest package (v4.7) (https://doi.org/10.1023/A:1010933404324), decision tree from the rpart package (v4.1) (10.32614/CRAN.package.rpart), support vector machine from the caret package, extreme gradient boosting (XGBoost) from the caret package, and LightGBM

from the lightgbm package (v4.6) (10.32614/CRAN.package.lightgbm). For each model, variable importance was derived from the respective regression coefficients. Predictors were ranked by importance, and the top 15 features were visualized using ggplot2 package (v4.0) (https://ggplot2.tidyverse.org). The same models were replicated in the KOBS cohort, consisting of the subcutaneous adipose tissue bulk RNA-seq of 259 bariatric patients (BMI>30 kg/m^2), where 22 individuals showed HO, and 219 were segregated as UO participants, as defined above.

RESULTS

Adipocytes in obesity show suppressed mitochondrial programs and altered lipid handling. To resolve cell-type-specific alterations associated with obesity, we performed multi-omic profiling of ex vivo adipocytes and EC sourced from the omental adipose tissue of 9 participants in the lean BMI range (BMI<25 kg/m²) and 8 participants living with obesity (BMI>30 kg/m²) (**Table S1**). We first focused on obesity-associated defects intrinsic to adipocytes. Untargeted LC–MS proteomics of isolated adipocytes (3 lean-range, 5 with obesity) identified ~1,400 protein groups retained for downstream analyses (**Figures S1a-b**). PCA (**Figure 1a**) and hierarchical clustering (**Figure S1c**) showed clear separation by BMI group. Using a significance cutoff of nominal p-value<0.05, a total of 459 proteins were identified as differentially abundant proteins (DAPs) by comparing proteomes of adipocytes from participants with obesity to those from lean participants, including 137 increased and 322 decreased proteins (**Figure 1b**). Enrichment analyses indicated that mitochondrial energy metabolism is the dominant axis suppressed in adipocytes in obesity. Over-representation analysis (ORA) and gene ontology (GO) highlighted downregulation of cellular and aerobic respiration and related energy-derivation processes, with cellular component enrichment mapping strongly to respiratory chain and mitochondrial complex structures (**Figure 1c** and **Table S7**). Consistently, Gene Set Enrichment Analysis (GSEA) using the Kyoto Encyclopedia of Genes and Genomes (KEGG) demonstrated negative enrichment of oxidative phosphorylation (OXPHOS), citrate (TCA) cycle, and valine/leucine/isoleucine degradation (adjusted p-value=4.73E-9), together with coordinated reductions in other mitochondrial substrate-handling pathways (**Figure 1d**). Reactome analyses further supported increased trafficking-related processes, including intra-Golgi and retrograde Golgi-to-ER transport (**Figure S1d**). Lipidomic profiling of isolated adipocytes was dominated (>99% of total lipid) by triglycerides (TG), necessitating relative rather than absolute quantification across lipid classes (**Figure 1e**). We identified 56 lipid species differing between groups. These TG species were preferentially depleted in adipocytes from participants living with obesity, whereas sphingomyelins (SM), phosphatidylethanolamines (PE), ether-linked phosphatidylcholines (PC O), phosphatidylcholines (PC), and diglycerides (DG) were relatively enriched (**Figure 1e**). Notably, TG species with shorter fatty acid chains (≤46 carbons total) and relatively higher saturation (≤3 double bonds) were less abundant in adipocytes from participants with obesity than in lean-range participants (**Figure 1f**). This compositional shift aligned with the proteomics data showing reduced abundance of enzymes supporting de novo fatty acid synthesis (e.g., PERC, FASN, ACACA) and mitochondrial β-oxidation (HADHA, HADHB, etc.) (**Figure 1b**), consistent with impaired lipid plasticity and oxidative capacity. On the other hand, metabolomics (**Figures S2a-c**) identified 30 metabolites differing between

groups (16 increased, 14 decreased). Metabolites increased in adipocytes from subjects with obesity included L-glutamic acid, glutathione, thiamine pyrophosphate, myo-inositol, N-acetylneuraminate, and L-carnitine, while several fatty acids were reduced (**Figures S2d**). In line with the proteomic results, fatty acid biosynthesis (6/29, p=4.1E-4) emerged as the most prominently altered process (**Figure S2e**). Together, these ex vivo data define an obesity-associated adipocyte state characterized by suppressed mitochondrial energy metabolism and remodelled TG distribution consistent with altered lipid handling.

EC in obesity exhibit reduced cell-cycle signaling and increased mitochondrial abundance. We next mapped obesity-associated changes in the adipose microvasculature by profiling adipose-resident EC from 7 lean-range participants (BMI<25 kg/m²) and 5 participants living with obesity (BMI>30 kg/m²) using flow cytometry/cell sorting and untargeted proteomics (**Figures S3a-b**). PCA (**Figure 2a**) and hierarchical clustering (**Figure S3c**) showed clear segregation by BMI group. We identified 439 DAP (nominal p-value<0.05), including 289 decreased and 150 increased proteins in EC from participants living with obesity (**Figure 2b**). Hallmark GSEA revealed enrichment of mitochondrial and lipid-handling programs in EC from participants with obesity, including OXPHOS (NES=2.36, p=1.23E-9), adipogenesis (NES=2.15, p=3.56E-7), and fatty acid metabolism (NES=1.48, p=4.51E-2), accompanied by downregulation of proliferation-associated pathways (i.e., E2F targets, G2M checkpoint, and Myc targets) and mTORC1 signalling (**Figure 2c**). Reactome analyses supported enrichment of insulin receptor signalling and aerobic respiration/electron transport (**Figure S3d**). Notably, several mitochondrial proteins suppressed in adipocytes from participants with obesity were regulated in the opposite direction in EC (**Figure 2d**), namely TCA cycle-related proteins (e.g., KYAT3, DLD, CYC1, PDHB, DLST, SUCLG2, ACAA2, ACAT1, NDUFAB1, MDH2, PPA2) and fatty acid β-oxidation proteins overlapping with branched-chain amino acid (BCAA) catabolism (DECR1, HADHA, HADHB) (**Figure 2e**). These data indicate a cell-type specific phenotype divergence in obesity: mitochondrial programs are suppressed in adipocytes yet enhanced at the protein level in adipose-resident EC, alongside reduced cell-cycle signalling.

MCM reproduces obesity-related adipocyte dysfunction and impairs mitochondrial respiration. To test whether inflammation is sufficient to induce the adipocyte phenotype observed in subjects with obesity, we exposed cultures of adipocytes to macrophage-conditioned media (MCM). As a technical prerequisite, we first verified expected proteome and lipidome remodelling during adipocyte differentiation (**Figures S4a-c**), confirming progressive enrichment of canonical adipocyte features encompassing significant alterations in lipidomes (**Figures S5a-f** and **Table S8**). We then modelled obesity-associated inflammatory stress by exposing differentiated adipocytes to MCM (**Figures S4d-f**). PCA on proteomic profiling data showed clear separation between control and MCM-treated adipocytes (**Figure 3a**). In fact, MCM altered 2,163 proteins (nominally p-value<0.05), including 1,218 decreased and 945 increased proteins (**Figure 3b**). ORA (GO) identified functional enrichment of mitochondrial metabolism as the dominant suppressed axis, including depletion of mitochondrial matrix, inner membrane, and respiratory complex components (**Figure 3c** and **Table S9**). KEGG GSEA (**Figure 3d**) further demonstrated coordinated downregulation of OXPHOS (NES=-2.47), BCAA degradation (NES=-2.36), carbon and propanoate metabolism, thermogenesis, and the citrate cycle (adjusted p-

value=2.24E-9). Functionally, MCM reduced oxygen consumption rate (OCR) in SGBS-derived adipocytes (**Figure S4g**), driven by impaired basal respiration (adjusted p-value=0.0054) and reduced ATP-linked respiration (adjusted p-value=0.0225). MCM also induced TG remodeling consistent with adipocyte dysfunction: decreased shorter, more saturated TG species, while longer, more unsaturated TG species were consistently increased (**Figures 3e-f**). Thus, macrophage-derived inflammatory signals are sufficient to reproduce key obesity-associated features in adipocytes, including suppression of mitochondrial pathways and coordinated lipid remodelling.

Immune and adipocyte-derived cues differentially shape EC adaptations. To dissect upstream signals contributing to the EC phenotype observed in obesity, we studied human adipose microvascular endothelial cells (HAMEC) under culture conditions modelling an obesity-like adipose milieu (**Figure 4a**). Exposure to MCM induced impaired respiration (**Figure 4b**), broad pathway disruption marked by inflammatory responses (e.g., interferon alpha/gamma response, TNFα signalling via NFκB, inflammatory response), and suppression of cell-cycle and bioenergetic pathways (**Figures S6a-g** and **Table S10**), together with reduced translation and altered extracellular matrix organization (**Figure 4c**). Functionally, MCM-treated EC displayed higher sprouting initiation, anchorage junctions, branching, and segment length (**Figure 4d**), consistent with endothelial remodelling compatible with endothelial–mesenchymal transition [55,56]. As the downregulation of mitochondrial proteins induced by MCM was in opposition to the increased mitochondrial protein abundance observed in EC from participants with obesity, we next tested whether adipocyte-derived cues contribute to the mitochondrial component of EC. Adipocyte-conditioned media (ACM) derived from MCM-activated adipocytes increased non-mitochondrial oxygen consumption, maximal OCR, ATP-linked respiration, and spare respiratory capacity in EC (**Figure 4e**). ACM induced 459 increased and 624 decreased proteins (nominal p-value<0.05) in HAMEC (**Figures S7a-e**), including mitochondrial protein fluctuations affecting biogenesis, organization, translation, ATP synthesis, and electron transfer (**Figures 4f** and **S7f**, and **Table S11**). ACM (but not MCM) also increased mitochondrial DNA content (**Figure 4g**), and coincided with repression of glycolysis (**Figure S7g**) and glycolytic proteins (**Figure S7e**), consistent with a shift toward mitochondrial energy production. Through GSEA of OXPHOS and Myc target-annotated proteins, we confirmed increased OXPHOS and decreased cell-cycle signalling in EC from participants with obesity (**Figure 4h**). While MCM treatments led to the downregulation of Myc target genes, mirroring the aforementioned observations, ACM functional measurements provided insights into the enrichment of mitochondrial proteins, supporting the dual impact of inflamed macrophages and adipocytes on EC dysfunction within the context of obesity. Together, these findings support a dual-source model of EC dysfunction in obesity: immune-cell inflammation shapes quiescence/angiogenic remodelling [57], whereas adipocyte-to-EC signalling may preferentially contribute to altered mitochondrial activity and respiration [58].

Surgery-induced weight loss remodels bulk adipose tissue toward mitochondrial activation and lipid plasticity. We next asked whether obesity-linked adipose programs recover (i.e., shift in the opposite direction) after sustained weight loss. We profiled paired abdominal adipose tissue from eighteen participants living with obesity before and after ~2 years of surgery-induced weight loss (**Table S2**).

Participants transitioned from class III obesity into the overweight range, with BMI decreasing from 42.8±4.9 to 28.6±5.5 kg/m² (p=9E-11) and fat mass from 55.7±7.0% to 39.5±7.3% (p=2.6E-10). As expected [59], HDL cholesterol increased from 54.7±14.1 to 74.9±24.1 mg/dl (p=9.9E-5). Untargeted in-depth LC–MS proteomics of the adipose tissue yielded 6,694 protein groups. After filtering (**Figures S8a-b**), 5,842 proteins were retained. Hierarchical clustering (**Figure S8c**) and PCA (**Figure 5a**) segregated samples by weight loss status. Comparing post-weight loss to baseline yielded 2,012 DAPs (nominal p-value<0.05), 1,154 increased and 858 decreased (**Figure 5b**). ORA (GO) showed strong enrichment of mitochondrial biological processes and components (**Figure 5c** and **Table S12**), including mitochondrial matrix and protein-containing complexes. KEGG GSEA indicated robust upregulation of mitochondrial and substrate-handling pathways after weight loss (**Figure 5d**), including valine/leucine/isoleucine degradation (NES=2.36, adjusted p-value=2.13E-8), TCA cycle (NES=2.32), OXPHOS (NES=2.3), pyruvate metabolism (NES=2.17), and fatty acid metabolism (NES=2.11). In parallel, inflammation-related signalling decreased, including complement/coagulation cascades, C-type lectin receptor signaling, and Toll-like receptor signalling (**Figure 5d**). Reactome GSEA further suggested normalization of COPI-mediated and Golgi–ER transport pathways (**Figure S8d**). On the other hand, lipidomics identified 122 lipid species significantly altered by weight loss (nominal p-value<0.05). Several membrane glycerophospholipid and sphingolipid classes increased, while free cholesterol and multiple DG species decreased (**Figure 5e**). TG remodeling was the most prominent shift: TG species with shorter fatty acids (≤47 carbons) and relatively higher saturation (≤3 double bonds) increased, whereas TG species with longer chains (≥50 carbons) decreased (**Figure 5f**). Integrating proteomics with lipidomics demonstrated concordant recovery of de novo lipogenic enzymes (ACLY, ACACA, FASN, etc.) and mitochondrial β-oxidation/BCAA metabolic process proteins (HADHA, HADHB, ACADM, etc.) alongside the TG shift, which was opposite in direction to observations in inflamed adipocyte cultures and ex vivo adipocytes isolated from participants living with obesity (**Figures S9a-c**). As this series of analysis profiled bulk adipose tissue rather than isolated cells, the post-weight loss signature likely reflects both adipocyte-intrinsic remodelling and changes in cellular composition and inflammatory activity within adipose tissue.

A robust adipocyte gene set emerges by intersecting obesity, inflammation, and weight loss-reversal across platforms. To pinpoint adipocyte determinants that consistently track dysfunction and its reversal, we intersected proteomic findings across (i) ex vivo isolated adipocytes in obesity, (ii) MCM-treated adipocytes in vitro, and (iii) bulk adipose tissue before and after weight loss. Proteins decreased in both adipocytes from participants with obesity and MCM-treated adipocytes but increased after weight loss comprised 177 candidates (**Figure 6a**). GO enrichment of this intersection highlighted mitochondrial processes and fatty acid metabolism remodelling, with mitochondrial cellular components dominating the signal (**Figure 6b**). To validate that these protein-level candidates generalize beyond our datasets and to benchmark directionality at the transcript level, we cross-referenced the 177 proteins against two independent transcriptomic resources (**Figure 6c**). In reference [60], adipose biopsies from 50 patients with obesity were profiled at baseline and 2 years after surgery-induced weight loss. In reference [61], O'Hara *et al*. profiled transcript changes in differentiated SGBS adipocytes [62] exposed to

14% MCM. Of the 177 candidates, 86 protein-coding transcripts recapitulated our directionality, i.e., upregulation correlated to adipose tissue shrinkage (**Figure 6d**), and downregulation when exposed to MCM (**Figure 6e**), presenting a core set enriched for mitochondrial function and BCAA metabolism. Conversely, proteins decreased after weight loss and/or increased in adipocytes from participants with obesity and/or in MCM-treated adipocytes comprised 156 candidates (**Figure 7a**). GO enrichment emphasized intracellular vesicle transport and cell–substrate junction pathways, with corresponding enrichment of vesicle coat/lumen and COPI-associated structures and adhesion-related binding functions (**Figure 7b**). Filtering these 156 candidates against transcripts downregulated with weight loss in bulk fat [60] and induced by MCM in adipocytes [61] yielded a refined list of 41 genes (**Figure 7c**), summarized by alluvial diagrams linking proteins to key pathways (**Figure 7d-e**). Notable components encode constituents of regulation of cell–substrate adhesion, cell adhesion molecule binding, extracellular exosome, and vesicle-mediated transport. Together, the 86 weight loss-reversible mitochondrial/BCAA-linked genes and the 41 vesicle/ adhesion-linked genes define a 127-gene signature that, in adipocytes/bulk fat, is consistently altered in obesity and inflammatory stress and shifts in the opposite direction with weight loss across platforms. A summary of proteomics data and study pipeline is provided in **Figure S10a**.

The adipocyte signature tracks metabolic vulnerability in independent cohorts and yields a 38-gene predictor of metabolic obesity. To connect the adipocyte signature to physiology at population scale, we re-analysed subcutaneous adipose RNA-seq data from three cohorts (**Figure S10b**): 335 unrelated male participants (median age 54 ± 5 years, BMI=26.8 ± 3.7 kg/m^2) from the Finnish METabolic Syndrome In Men (METSIM) cohort [27,28] (**Table S3**), 49 BMI-discordant monozygotic twin pairs (Finnish Twin Cohort) [29], and 451 adults living with obesity (31% men; median age 46 ± 10 years, BMI=46.8 ± 7.9 kg/m^2) from the multi-centered Spanish ADIPOMIT cohort [30] (**Table S4**). In METSIM, we tested associations with BMI, HDL cholesterol, fasting TG, and blood glucose after adjusting for BMI, age, and type 2 diabetes (**Figure 8a**). This benchmarking study gave us an overview of our previous meta-associations in a sample representing a male population prone to cardiometabolic complications, exceeding those in females [63]. In BMI-discordant twins, 95 of the 127 candidates (74.8%) were differentially expressed (FDR adjusted p-value<0.05) in the heavier co-twin (**Figure 8b**), supporting their link to adiposity independent of genetic background. In ADIPOMIT, meta-analysis of gene–trait associations (**Figure 8c**) showed that only 60 candidates (47%) correlated with BMI (nominal p-value<0.05), whereas in METSIM 115 candidates (91%) did so. We next assessed whether the 127-gene signature stratifies metabolic vulnerability among people living with obesity in ADIPOMIT. Individuals with one or more metabolic abnormalities (i.e., dyslipidemia, hypertriglyceridemia, and hyperglycemia) were classified as “unhealthy” obese (UO), and those with none as “healthy” obese (HO). Using the single-sample Gene Set Enrichment Analysis (ssGSEA) algorithm [64], a gene-set score per sample associated with comorbidity presence (**Figure 8d**) and distinguished HO from UO with an AUC of 0.7 (0.63–0.77) (**Figure 8e**). Stepwise regression including age, sex, and Log_2(BMI) as covariates selected 38 genes (**Figure 8f**) that substantially improved discrimination (**Figures 8g-h**), yielding an AUC of 0.92 (0.89–0.95). Thus, the adipocyte signature not

only tracks obesity and inflammation across datasets but also captures clinically relevant metabolic vulnerability among people living with obesity.

Integrating adipocyte and endothelial gene candidates yields a broader genomic signature of cardiometabolic vulnerability. We next extended the framework to include EC-associated protein patterns linked to obesity-related meta-inflammation (**Figures S11a-b**). Integrative analysis of adipose-resident EC and HAMEC cultures yielded 237 proteins with patterns negatively correlating with obesity (**Figure 9a**) and 91 proteins defining an inflamed EC phenotype (**Figure 9b**). Using funnel-diagram pipelines, we shortlisted EC features that replicate weight loss-associated expression patterns in bulk adipose transcriptomes [29,60,65], generating a set of 34 EC genes (19+15) mostly associated with protein translation and endo/lysosome function (**Figures S12a-c**), consistent with dysregulated protein synthesis and compromised lysosomal degradation in obesity/inflammation. However, when queried in the ADIPOMIT cohort, this EC-type-resolved gene signature showed limited correlation with metabolic comorbidities (**Figure 9c** and **Figure S12d**). Next, forward/backward stepwise AIC selection across 159 protein candidates (125 adipocyte-specific and 32 EC-derived genes, plus 2 common proteins, as shown in **Figure S12e**) identified in this study yielded a new model including 36 adipocyte-derived and 10 EC-derived genes (**Figures 9d**); a refined, final 46-gene predictor signature capturing metabolic distress in subjects with obesity with an AUC of 0.95 (0.92–0.97) (**Figure 9e**). Notably, across six machine learning algorithms distinguishing UO from HO, both adipocyte (ACADSB, BCAT1, BCKDHB, CBR4, CD163, CKB, CPPED1, DLST, FASN, IVD, LCP1, LMNB1, LPXN, MIF, NCEH1, NDUFA5, PDHX, PECR, PTPRJ, SERPINB8, and SHMT1) and EC genes (CALU, CTSS, and RPS4X), together with BMI (Log_2 BMI), consistently ranked among the top contributors for metabolic obesity in the ADIPOMIT cohort (**Figure S13a**). To replicate our findings on an independent sample of individuals with obesity, we utilized, as defined above, the Kuopio OBesity Surgery (KOBS) dataset [4]. This confirmatory study of bulk subcutaneous adipose tissue RNA-seq conducted in 259 bariatric patients, where 22 individuals showed HO, and 219 were segregated in UO participants (**Table S5**), validated our 46-gene signature (**Figure 9f**) with an AUC of 0.93 (0.88–0.99) (**Figure 9g**), while machine learning algorithms (**Figure S13b**) further confirmed the apparent relevance of at least 15 adipocyte and EC-related gene candidates (including BCAT1, CALU, CDK6, COQ9, CPPED1, CTSS, DLD, NDUFA5, NRP2, PCCA, PECR, SEC16A, SHMT1, UCHL3, and UQCRC2) in defining metabolic obesity across different datasets (**Figure S13c**). Collectively, our findings connect altered adipocyte and EC protein landscapes to bulk adipose genomics, and support a cell-informed signature that helps addressing cardiometabolic vulnerability in people living with obesity.

DISCUSSION

Obesity is accompanied by adipose tissue dysfunction linking excessive adiposity to metabolic disease, yet the programs responsible are difficult to attribute to specific cell types and distinguish in experimental settings from changes accompanying weight loss. Here, we used a layered design to (i) define obesity-associated, cell-type-resolved molecular phenotypes in adipocytes and EC, (ii) mimic an obesity-like inflammatory milieu in vitro, probing macrophage-adipocyte-endothelial signalling using

MCM and ACM, and (iii) determine which obesity-associated proteins show evidence of recovery in bulk adipose tissue after weight loss. The resulting protein signatures of obesity and inflammation were then intersected with transcriptomic datasets of weight loss [60] and inflamed adipocytes [61], and evaluated for physiological relevance across several human cohorts (METSIM [28], BMI-discordant twins [29], ADIPOMIT [30], and KOBS [4]), yielding a refined, non-immune cell-derived 46-gene predictor of metabolic vulnerability in people with obesity. Together, these findings support a model in which obesity-associated adipocyte dysfunction is primarily inflammation-responsive, and shows evidence of reversibility with weight loss, while microvascular EC phenotypes reflect distinct and context-dependent cues within the adipose microenvironment, able to capture together the whole-body metabolic status. A diagram summarizing our research and main conclusions is presented in **Figure 10**.

Our integrative approach confirmed mitochondrial malfunction as a prominent feature of obesity, marked by a significant impairment of adipocyte respiration and normalized upon weight loss [66]. This reinforces the notion that adipose tissue alterations predominantly reflect pathological cues occurring within adipocytes [67]. Replication in adipocyte cultures when challenged with macrophage-derived cytokines further supports a pivotal role of immune inflammation and macrophage-to-adipocyte communication [68,69]. Conversely, intersection of proteins exhibiting an inverse pattern (i.e., decreased in adipose tissue upon weight loss and more abundant in obese/inflamed adipocytes) highlighted vesicle transport and cell-substrate junctions. The former aligns with the increased secretion of obese, inflamed adipocytes, reflecting altered endocrine function and stress adaptation [70,71]. Notably, major coatomer components critical for endoplasmic reticulum-Golgi vesicle trafficking were identified (CLTC, COTL1, COPG1, COPB2, etc.), further corroborating a connection between obesity and the synthesis and release of extracellular vesicles [72], which is alleviated after significant weight loss [73]. The overrepresentation of cell-substrate components of junctional complexes is also consistent with reports on mechanophysical interactions with the extracellular matrix (ECM), contributing to adipose tissue remodelling in obesity [74,75]. For instance, dynamic mediators of adipose cell adhesion, such as adipocyte adhesion molecule (e.g., ACAM), can control the development of obesity [76], while modification of focal adhesions deeply impacts the adipogenic transformation of mesenchymal stem cells [77,78], and deletion of integrin-mediated cell adhesion proteins such as integrin-β1 (ITGB1) [79] and kindlin-2 (FERMT2) [80] alters adipocyte function, accompanying excessive adiposity.

Next, by intersecting our findings with publicly available transcriptomes characterising adipose tissue upon weight loss [60] and adipocyte inflammation [61], we shortlisted 127 genes consistently altered in “obese” adipocytes, on the transcript and protein levels, both. The clinical relevance of these biomarkers was supported by their associations with metabolic distress, including dyslipidaemia, hypertriglyceridemia, and hyperglycaemia across two independent human cohorts (METSIM [35] and ADIPOMIT [30]) and a cross-sectional study conducted in BMI-discordant twins [29]. Refinement using stepwise regression analysis yielded a core set of 38 genes that, when combined, substantially enhanced diagnostic capacity for assessing gene-trait associations and the risk of metabolic disruption

in subjects with obesity. This set of gene products represents, in adipocytes, a promising target, not only for extending our mechanistic understanding of the pathophysiology of obesity, but also for guiding the development of novel diagnostic tools and therapeutic interventions aimed at mitigating the comorbidities of obesity.

In this context, significant alterations in lipid signatures have proven important in tackling adipose tissue function and energy handling [81]. In our complementary approaches, a reduction in TG with comparatively short, saturated fatty acid chains was observed in adipocytes under obese and inflammatory conditions, while being enriched in adipose tissue upon weight loss. In human adipocytes, the relevant fatty acid chains are largely derived from *de novo* lipogenesis (DNL) [82]. Our finding aligns with previous observations [81], and corroborates diminished DNL in obese/inflamed adipocytes, also reflected in the depletion of major DNL enzymes in our proteomic data. Moreover, a reduction in long-chain, polyunsaturated fatty acid (PUFA)-containing TG species upon weight loss coincides with an increase upon pro-inflammatory treatments on primary adipocytes. This replicates studies reporting elevated PUFA in the adipose tissue of subjects with obesity and type 2 diabetes patients [81,83], as well as mice on high fat diets [84]. The enrichment of PUFA-containing TG species raises questions on how and why distinct TG are generated in adipocytes, and whether they play relevant roles in the development of metabolic disturbances. Interestingly, a PUFA subset (derived from ω-6 PUFA) is considered pro-inflammatory, while others (obtained from both ω-3 and ω-6 PUFA) contribute to the resolution of innate immune activation in adipose tissue [73,85].

On the other hand, the proteomic profiling of adipose-resident EC in individuals with obesity hinted at a quiescent phenotype, characterized by low abundance of cell cycle-related proteins and consistent with the reduced vasculature and angiogenic capacity of hyperplastic fat pads [14,86]. Paradoxically, enhanced mitochondrial activity and fatty acid oxidation were also observed in “obese” EC. This may be due to the enhanced availability of fatty acids, known to leak out from hypertrophic, insulin-resistant adipocytes [87,88]. Of note, respiratory chain components were also elevated in “obese” EC, putatively yielding excessive production of Reactive Oxygen Species (ROS). The resulting oxidative stress can induce EC dysfunction, leading to the sustained activation and increased adhesion of immune cells, while contributing to the leakiness of vascular walls [89,90], perpetuating adipose tissue inflammation. As EC mostly rely on glycolysis for energy production [91,92], the upregulation of mitochondrial components likely underscores a change in cellular energetics reflecting quiescent EC, which employ FA oxidation and the TCA cycle to support cellular redox balance against oxidative damage [93].

Interestingly, while the treatment of EC cultures with MCM recapitulated the reduction of cell cycle-related proteins accompanying inflammatory activation, the overrepresentation of proteins related to mitochondrial function did not, suggesting the secretome of “obese” adipocytes to be required for full induction of the obese phenotype in adipose-resident EC. Indeed, exposure of EC to media conditioned with inflamed adipocytes (ACM) resulted in increased abundance of several proteins related to mitochondrial respiration and boosted oxygen consumption, together with pathway alterations also

observed in “obese” EC and MCM-treated HAMEC. Collectively, these data support the view that pro-inflammatory signals from activated macrophages are crucial for adipose tissue dysfunction, both (i) altering adipocyte lipid and energy metabolism, vesicle transport and adhesion properties, while (ii) reprogramming EC energy metabolism through the influence of inflamed adipocytes with far reaching consequences in adipose tissue [94,95].

This study encompasses several strengths. First, we employed ex vivo, in vitro and in vivo approaches and their cross-section to identify protein and lipid signatures skewed by obesity and inflammation. Second, the inclusion of adipocytes and EC broadens the examination of the impact of excess weight, inflammation, weight loss, and other obesity-related outcomes across two of the most relevant adipose-resident, non-immune cell types. Third, we solidified the findings by filtering protein patterns against transcriptomic studies, yielding highly credible lists of genes/proteins dysregulated in obesity. In addition, by using four independent human cohorts, we carefully shortlisted our cell signatures against a comprehensive range of obesity-related outcomes to disentangle the most significant cell-resolved molecular phenotypes of metabolic vulnerability in subjects with obesity, assessing not only the association with adiposity, but also their capacity to predict metabolic outcomes with very convincing results (ROC curves>0.9).

However, there are also limitations to consider. These include the descriptive nature of this study, as well as the modest sample size employed for the initial omics analyses, which substantially limits statistical power. In addition, we lacked precise data on some potential confounding variables, and our study cohorts focus on white European individuals between the ages of 40 to 70. Therefore, caution should be applied when extrapolating our findings to other populations. However, in many other ways, the multiple transcriptomic cohorts queried, when levelled by means of cell-type-resolved and bulk fat protein profiles, hit cross-validation at both protein and mRNA levels, adding confidence in the robustness of our main conclusions. Overall, although our data cannot offer causal insight, the current study constitutes a resource to guide future experimental investigations of protein and lipid targets with an impact on the welfare of bona fide adipose-resident cells and adipose welfare.

Declarations

DATA AVAILABILITY

The source data underlying the findings of this study has been deposited in public data repositories, and/or is presented as a Source Data file with the manuscript. Protein raw data, processing and statistical analysis can be accessed at the ProteomeXchange Consortium via the MassIVE partner repositories (http://proteomecentral.proteomexchange.org) with the following identifier: PXD070733 (MassIVE ID: MSV000099905), under the accession DOI number *10.25345/C54Q7R37G*. The lipidomic data of human adipose tissue and ex vivo isolated adipocytes has been made publicly available in the Figshare repository, under accession DOI number *10.6084/m9.figshare.28638761*. Data on human

preadipocyte cultures differentiated into adipocytes and treated with MCM-induced inflammatory conditions is available under accession DOI number *10.6084/m9.figshare.25541005*. Additional datasets used during this research are publicly available in the GEO repository under the following accession codes: GSE199063 [60], GSE14312 [61], and GSE53378 [65].

AUTHOR CONTRIBUTIONS

All authors revised the manuscript. V.C., L.L., A.L., D.D.P., and S.P. managed the daily experiments, researched the data, and performed the statistical analysis. A.F-S., P.A.N.H., and J.M.M-N. assisted with experimental handling, and data collection and analysis. J.I.R-H., E.P-S., J.H., K.H.P., and J.M.F-R. coordinated human samples, clinical information and intellectual content collection. A.K., M.L., and P.P. coordinated intellectual content collection and statistical analysis in the METSIM study dataset. G.F., O.A.R-Z., F.J.T., C.D., and J.M.F-R. granted access to the ADIPOMIT study dataset. V.M., J.P., M.U.K., and P.P. coordinated intellectual content collection and statistical confirmation of results in the KOBS cohort. A.L., R.B., M.H., and G.L. conducted quantitative lipidomics. W.S., J.G., M.G.-S., S.K., and M.V. carried out the proteomic analyses. Y.Z., V.M.O., and F.J.O. researched the data and performed statistical analyses. V.M.O. and F.J.O. conceived and supervised the study, designed the research, guided the interpretation of results, wrote the manuscript, and secured funding.

ACKNOWLEDGMENTS

This work was supported by the research grant PI21/00074 (F.J.O.), cofounded by the Instituto de Salud Carlos III (ISCIII), the European Regional Development Fund (ERDF) “a way to build Europe”, and the European Social Fund (ESF), “investing in your future”, by the Fondo Europeo de Desarrollo Regional (FEDER), the Agencia Estatal de Investigación, Ministerio de Ciencia, Innovación y Universidades, Gobierno de España (CNS2023-145394 to F.J.O.), and by the Academy of Finland (grant 322647 to V.M.O.). V.M.O. was also recipient of grants from the Sigrid Juselius Foundation, Medicinska Understödsföreningen Liv och Hälsa, the Finnish Diabetes Research Foundation, and the Finnish Society of Sciences and Letters. V.C. received grants from the Yrjö Jahnsson Foundation, and the Ministry of Education in Finland (EDUFI). F.J.O. (MS19/00109) was recipient of the Miguel Servet scheme (ISCIII). V.C. is employee in the Doctoral Programme of Clinical Research, University of Helsinki. A.L. (FI19/00045, MV22/00074) was recipient of a “Contrato Predoctoral de Formación en Investigación en Salud” (PFIS, ISCIII), and a “Movilidad de personal investigador contratado en el marco de la AES” (M-AES). This research was also supported by the Deutsche Forschungsgemeinschaft (DFG, German Research Foundation – 416910386 GRK 2573), and the Deutsche Krebshilfe (Grant No. 70116773) (to M.G.-S.). P.P. and M.U.K. were supported by NIH grant 1R01HL170604. M.U.K. was also supported by Sigrid Juselius Foundation and the Finnish Foundation for Cardiovascular Research. We want to acknowledge the collaboration of all the participants involved in this study, the FATBANK platform (also promoted by the CIBEROBN), and the Biobanc (B.0000872) of the Institut d’Investigació Biomèdica de Girona (IDIBGI), integrated in the Spanish National Biobanks Network. We also want to thank the CERCA and PERIS (SLT028/23/000133) programs (Generalitat de Catalunya) for financial support. We are

grateful to Alexandre Santos, Tiisa Kalske, Anna-Maria Thölix, Antti Turunen, Henrik Husu, Henriikka Hietaniemi, Pauliina Reijonen, Tuula Ranta-Knuuttila, Minna Räsänen, Rohit Verma, Leopold Nelimarkka and Panu Aaltonen for providing the adipose tissue biopsies of gallstone patients. Riikka Kosonen and Mareike Rohrbach are thanked for technical assistance. Moreover, we warmly thank the HiLIFE Biomedicum Flow cytometry unit at the University of Helsinki.

COMPETING INTERESTS

The authors declare no competing interests concerning this study. All authors have participated in the execution and analysis of the study, are aware of and agree to the content of the manuscript. The contents of this manuscript have not been copyrighted or published previously, nor are under consideration for publication elsewhere.

References

1. Boutari C, Mantzoros CS. A 2022 update on the epidemiology of obesity and a call to action: as its twin COVID-19 pandemic appears to be receding, the obesity and dysmetabolism pandemic continues to rage on. *Metabolism* 2022; **133**: 155217.
2. Blüher M. Obesity: global epidemiology and pathogenesis. *Nat Rev Endocrinol* 2019; **15**: 288–298.
3. Kahn CR, Wang G, Lee KY. Altered adipose tissue and adipocyte function in the pathogenesis of metabolic syndrome. *J Clin Invest* 2019; **129**: 3990–4000.
4. van der Kolk BW, Muniandy M, Kaminska D, Alvarez M, Ko A, Miao Z *et al.* Differential Mitochondrial Gene Expression in Adipose Tissue Following Weight Loss Induced by Diet or Bariatric Surgery. *J Clin Endocrinol Metab* 2021; **106**: 1312–1324.
5. Heinonen S, Buzkova J, Muniandy M, Kaksonen R, Ollikainen M, Ismail K *et al.* Impaired Mitochondrial Biogenesis in Adipose Tissue in Acquired Obesity. *Diabetes* 2015; **64**: 3135–3145.
6. Rosen ED, Spiegelman BM. What we talk about when we talk about fat. *Cell* 2014; **156**: 20–44.
7. Kusminski CM, Bickel PE, Scherer PE. Targeting adipose tissue in the treatment of obesity-associated diabetes. *Nat Rev Drug Discov* 2016; **15**: 639–660.
8. Sakers A, De Siqueira MK, Seale P, Villanueva CJ. Adipose-tissue plasticity in health and disease. *Cell* 2022; **185**: 419–446.
9. Smith GI, Mittendorfer B, Klein S. Metabolically healthy obesity: facts and fantasies. *J Clin Invest* 2019; **129**: 3978–3989.
10. Blüher M. Metabolically Healthy Obesity. *Endocr Rev* 2020; **41**: bnaa004.
11. Gregor MF, Hotamisligil GS. Inflammatory mechanisms in obesity. *Annu Rev Immunol* 2011; **29**: 415–445.
12. Russo L, Lumeng CN. Properties and functions of adipose tissue macrophages in obesity. *Immunology* 2018; **155**: 407–417.

13. Ghaben AL, Scherer PE. Adipogenesis and metabolic health. *Nat Rev Mol Cell Biol* 2019; **20**: 242–258.
14. Crewe C, An YA, Scherer PE. The ominous triad of adipose tissue dysfunction: inflammation, fibrosis, and impaired angiogenesis. *J Clin Invest* 2017; **127**: 74–82.
15. de Zeeuw P, Wong BW, Carmeliet P. Metabolic adaptations in diabetic endothelial cells. *Circ J* 2015; **79**: 934–941.
16. Crandall DL, Hausman GJ, Kral JG. A review of the microcirculation of adipose tissue: anatomic, metabolic, and angiogenic perspectives. *Microcirculation* 1997; **4**: 211–232.
17. Rojas-Rodriguez R, Gealekman O, Kruse ME, Rosenthal B, Rao K, Min S *et al.* Adipose tissue angiogenesis assay. *Methods Enzymol* 2014; **537**: 75–91.
18. Oikonomou EK, Antoniades C. The role of adipose tissue in cardiovascular health and disease. *Nat Rev Cardiol* 2019; **16**: 83–99.
19. Graupera M, Claret M. Endothelial Cells: New Players in Obesity and Related Metabolic Disorders. *Trends Endocrinol Metab* 2018; **29**: 781–794.
20. Goossens GH, Bizzarri A, Venteclef N, Essers Y, Cleutjens JP, Konings E *et al.* Increased adipose tissue oxygen tension in obese compared with lean men is accompanied by insulin resistance, impaired adipose tissue capillarization, and inflammation. *Circulation* 2011; **124**: 67–76.
21. Draoui N, de Zeeuw P, Carmeliet P. Angiogenesis revisited from a metabolic perspective: role and therapeutic implications of endothelial cell metabolism. *Open Biol* 2017; **7**: 170219.
22. Rupnick MA, Panigrahy D, Zhang C-Y, Dallabrida SM, Lowell BB, Langer R *et al.* Adipose tissue mass can be regulated through the vasculature. *Proc Natl Acad Sci U S A* 2002; **99**: 10730–10735.
23. Corvera S, Gealekman O. Adipose tissue angiogenesis: impact on obesity and type-2 diabetes. *Biochim Biophys Acta* 2014; **1842**: 463–472.
24. Sorop O, Olver TD, van de Wouw J, Heinonen I, van Duin RW, Duncker DJ *et al.* The microcirculation: a key player in obesity-associated cardiovascular disease. *Cardiovasc Res* 2017; **113**: 1035–1045.
25. Tang W, Zeve D, Suh JM, Bosnakovski D, Kyba M, Hammer RE *et al.* White fat progenitor cells reside in the adipose vasculature. *Science* 2008; **322**: 583–586.
26. Chaurasiya V, Pham DD, Harju J, Juuti A, Penttilä A, Emmagouni SKG *et al.* Human visceral adipose tissue microvascular endothelial cell isolation and establishment of co-culture with white adipocytes to analyze cell-cell communication. *Exp Cell Res* 2023; **433**: 113819.
27. Laakso M, Kuusisto J, Stančáková A, Kuulasmaa T, Pajukanta P, Lusis AJ *et al.* The Metabolic Syndrome in Men study: a resource for studies of metabolic and cardiovascular diseases. *J Lipid Res* 2017; **58**: 481–493.
28. Pan DZ, Garske KM, Alvarez M, Bhagat Y V, Boocock J, Nikkola E *et al.* Integration of human adipocyte chromosomal interactions with adipose gene expression prioritizes obesity-related genes from GWAS. *Nat Commun* 2018; **9**: 1512.

29. van der Kolk BW, Saari S, Lovric A, Arif M, Alvarez M, Ko A *et al.* Molecular pathways behind acquired obesity: Adipose tissue and skeletal muscle multiomics in monozygotic twin pairs discordant for BMI. *Cell reports Med* 2021; **2**: 100226.
30. Paulí S, Oliveras-Cañellas N, Moreno-Navarrete JM, Castells-Nobau A, Ortega FJ, Rodriguez-Hermosa JI *et al.* Cellular composition and transcriptomics of subcutaneous adipose tissue linked to blood glycated haemoglobin. *Eur J Clin Invest* 2025; **55**: e70033.
31. Wessel D, Flügge UI. A method for the quantitative recovery of protein in dilute solution in the presence of detergents and lipids. *Anal Biochem* 1984; **138**: 141–143.
32. Yu F, Teo GC, Kong AT, Fröhlich K, Li GX, Demichev V *et al.* Analysis of DIA proteomics data using MSFragger-DIA and FragPipe computational platform. *Nat Commun* 2023; **14**: 4154.
33. Gómez-Serrano M, Camafeita E, García-Santos E, López JA, Rubio MA, Sánchez-Pernaute A *et al.* Proteome-wide alterations on adipose tissue from obese patients as age-, diabetes- and gender-specific hallmarks. *Sci Rep* 2016; **6**: 25756.
34. Hughes CS, Moggridge S, Müller T, Sorensen PH, Morin GB, Krijgsveld J. Single-pot, solid-phase-enhanced sample preparation for proteomics experiments. *Nat Protoc* 2019; **14**: 68–85.
35. Ritchie ME, Phipson B, Wu D, Hu Y, Law CW, Shi W *et al.* Limma powers differential expression analyses for RNA-sequencing and microarray studies. *Nucleic Acids Res* 2015; **43**: e47.
36. Yu G, Wang L-G, Han Y, He Q-Y. clusterProfiler: an R package for comparing biological themes among gene clusters. *OMICS* 2012; **16**: 284–287.
37. BLIGH EG, DYER WJ. A rapid method of total lipid extraction and purification. *Can J Biochem Physiol* 1959; **37**: 911–917.
38. Liebisch G, Lieser B, Rathenberg J, Drobnik W, Schmitz G. High-throughput quantification of phosphatidylcholine and sphingomyelin by electrospray ionization tandem mass spectrometry coupled with isotope correction algorithm. *Biochim Biophys Acta - Mol Cell Biol Lipids* 2004; **1686**: 108–117.
39. Liebisch G, Drobnik W, Lieser B, Schmitz G. High-throughput quantification of lysophosphatidylcholine by electrospray ionization tandem mass spectrometry. *Clin Chem* 2002; **48**: 2217–2224.
40. Matyash V, Liebisch G, Kurzchalia T V, Shevchenko A, Schwudke D. methods Lipid extraction by methyl-tert-butyl ether for high-throughput lipidomics. *J Lipid Res* 2008; **49**: 1137–1146.
41. Liebisch G, Drobnik W, Reil M, Trümbach B, Arnecke R, Olgemöller B *et al.* Quantitative measurement of different ceramide species from crude cellular extracts by electrospray ionization tandem mass spectrometry (ESI-MS/MS). *J Lipid Res* 1999; **40**: 1539–46.
42. Zemski Berry KA, Murphy RC. Electrospray ionization tandem mass spectrometry of glycerophosphoethanolamine plasmalogen phospholipids. *J Am Soc Mass Spectrom* 2004; **15**: 1499–1508.
43. Scherer M, Schmitz G, Liebisch G. Simultaneous quantification of cardiolipin, bis(monoacylglycero)phosphate and their precursors by hydrophilic interaction LC-MS/MS including

correction of isotopic overlap. *Anal Chem* 2010; **82**: 8794–8799.

44. Höring M, Ejsing CS, Krautbauer S, Ertl VM, Burkhardt R, Liebisch G. Accurate quantification of lipid species affected by isobaric overlap in Fourier-Transform mass spectrometry. *J Lipid Res* 2021; **62**: 100050.
45. Höring M, Ejsing CS, Hermansson M, Liebisch G. Quantification of Cholesterol and Cholesteryl Ester by Direct Flow Injection High-Resolution Fourier Transform Mass Spectrometry Utilizing Species-Specific Response Factors. *Anal Chem* 2019; **91**: 3459–3466.
46. Liebisch G, Binder M, Schifferer R, Langmann T, Schulz B, Schmitz G. High throughput quantification of cholesterol and cholesteryl ester by electrospray ionization tandem mass spectrometry (ESI-MS/MS). *Biochim Biophys Acta - Mol Cell Biol Lipids* 2006; **1761**: 121–128.
47. Zhou Y, Orešič M, Leivonen M, Gopalacharyulu P, Hyysalo J, Arola J *et al.* Noninvasive Detection of Nonalcoholic Steatohepatitis Using Clinical Markers and Circulating Levels of Lipids and Metabolites. *Clin Gastroenterol Hepatol Off Clin Pract J Am Gastroenterol Assoc* 2016; **14**: 1463-1472.e6.
48. Schindelin J, Arganda-Carreras I, Frise E, Kaynig V, Longair M, Pietzsch T *et al.* Fiji: an open-source platform for biological-image analysis. *Nat Methods* 2012; **9**: 676–682.
49. Kanehisa M, Goto S. KEGG: kyoto encyclopedia of genes and genomes. *Nucleic Acids Res* 2000; **28**: 27–30.
50. Ashburner M, Ball CA, Blake JA, Botstein D, Butler H, Cherry JM *et al.* Gene ontology: tool for the unification of biology. The Gene Ontology Consortium. *Nat Genet* 2000; **25**: 25–29.
51. Wei D, González-Marrachelli V, Melgarejo JD, Liao C-T, Hu A, Janssens S *et al.* Cardiovascular risk of metabolically healthy obesity in two european populations: Prevention potential from a metabolomic study. *Cardiovasc Diabetol* 2023; **22**: 82.
52. Blüher M. The distinction of metabolically 'healthy' from 'unhealthy' obese individuals. *Curr Opin Lipidol* 2010; **21**: 38–43.
53. Robin X, Turck N, Hainard A, Tiberti N, Lisacek F, Sanchez J-C *et al.* pROC: an open-source package for R and S+ to analyze and compare ROC curves. *BMC Bioinformatics* 2011; **12**: 77.
54. Topçuoğlu BD, Lapp Z, Sovacool KL, Snitkin E, Wiens J, Schloss PD. mikropml: User-Friendly R Package for Supervised Machine Learning Pipelines. *J open source Softw* 2021; **6**: 3073.
55. Pedersen TO, Blois AL, Xue Y, Xing Z, Sun Y, Finne-Wistrand A *et al.* Mesenchymal stem cells induce endothelial cell quiescence and promote capillary formation. *Stem Cell Res Ther* 2014; **5**: 23.
56. Chavkin NW, Vippa T, Jung C, McDonnell S, Hirschi KK, Gokce N *et al.* Obesity accelerates endothelial-to-mesenchymal transition in adipose tissues of mice and humans. *Front Cardiovasc Med* 2023; **10**: 1264479.
57. Xiao W, Oldham WM, Priolo C, Pandey AK, Loscalzo J. Immunometabolic Endothelial Phenotypes: Integrating Inflammation and Glucose Metabolism. *Circ Res* 2021; **129**: 9–29.

58. Crewe C, Funcke J-B, Li S, Joffin N, Gliniak CM, Ghaben AL *et al.* Extracellular vesicle-based interorgan transport of mitochondria from energetically stressed adipocytes. *Cell Metab* 2021; **33**: 1853-1868.e11.
59. Nienov OH, Machado FD, Dias LS, De Carli LA, Schmid H. Effect of Bariatric Surgery on High-Density Lipoprotein (HDL) Cholesterol in Non-diabetic Patients with Severe Obesity. *Obes Surg* 2020; **30**: 154–160.
60. Kerr AG, Andersson DP, Rydén M, Arner P, Dahlman I. Long-term changes in adipose tissue gene expression following bariatric surgery. *J Intern Med* 2020; **288**: 219–233.
61. O'Hara A, Lim FL, Mazzatti DJ, Trayhurn P. Microarray analysis identifies matrix metalloproteinases (MMPs) as key genes whose expression is up-regulated in human adipocytes by macrophage-conditioned medium. *Pflugers Arch Eur J Physiol* 2009; **458**: 1103–1114.
62. Wabitsch M, Brenner RE, Melzner I, Braun M, Möller P, Heinze E *et al.* Characterization of a human preadipocyte cell strain with high capacity for adipose differentiation. *Int J Obes Relat Metab Disord J Int Assoc Study Obes* 2001; **25**: 8–15.
63. Gerdts E, Regitz-Zagrosek V. Sex differences in cardiometabolic disorders. *Nat Med* 2019; **25**: 1657–1666.
64. Barbie DA, Tamayo P, Boehm JS, Kim SY, Moody SE, Dunn IF *et al.* Systematic RNA interference reveals that oncogenic KRAS-driven cancers require TBK1. *Nature* 2009; **462**: 108–112.
65. Ortega FJ, Mercader JM, Moreno-Navarrete JM, Nonell L, Puigdecanet E, Rodriquez-Hermosa JI *et al.* Surgery-induced weight loss is associated with the downregulation of genes targeted by MicroRNAs in adipose tissue. *J Clin Endocrinol Metab* 2015; **100**. doi:10.1210/jc.2015-2357.
66. van der Kolk BW, Pirinen E, Nicoll R, Pietiläinen KH, Heinonen S. Subcutaneous adipose tissue and skeletal muscle mitochondria following weight loss. *Trends Endocrinol Metab* 2025; **36**: 339–363.
67. Reinisch I, Ghosh A, Noé F, Sun W, Dong H, Leary P *et al.* Unveiling adipose populations linked to metabolic health in obesity. *Cell Metab* 2025; **37**: 640-655.e4.
68. Weisberg SP, McCann D, Desai M, Rosenbaum M, Leibel RL, Ferrante AWJ. Obesity is associated with macrophage accumulation in adipose tissue. *J Clin Invest* 2003; **112**: 1796–1808.
69. Hotamisligil GS. Inflammation, metaflammation and immunometabolic disorders. *Nature* 2017; **542**: 177–185.
70. Tilg H, Moschen AR. Adipocytokines: Mediators linking adipose tissue, inflammation and immunity. *Nat Rev Immunol* 2006. doi:10.1038/nri1937.
71. Matilainen J, Berg V, Vaittinen M, Impola U, Mustonen A-M, Männistö V *et al.* Increased secretion of adipocyte-derived extracellular vesicles is associated with adipose tissue inflammation and the mobilization of excess lipid in human obesity. *J Transl Med* 2024; **22**: 623.
72. Samuelson I, Vidal-Puig AJ. Fed-EXosome: extracellular vesicles and cell-cell communication in metabolic regulation. *Essays Biochem* 2018; **62**: 165–175.

73. Soták M, Clark M, Suur BE, Börgeson E. Inflammation and resolution in obesity. *Nat Rev Endocrinol* 2025; **21**: 45–61.
74. Henegar C, Tordjman J, Achard V, Lacasa D, Cremer I, Guerre-Millo M *et al.* Adipose tissue transcriptomic signature highlights the pathological relevance of extracellular matrix in human obesity. *Genome Biol* 2008; **9**: R14.
75. Sun K, Kusminski CM, Scherer PE. Adipose tissue remodeling and obesity. *J Clin Invest* 2011; **121**: 2094–2101.
76. Murakami K, Eguchi J, Hida K, Nakatsuka A, Katayama A, Sakurai M *et al.* Antiobesity Action of ACAM by Modulating the Dynamics of Cell Adhesion and Actin Polymerization in Adipocytes. *Diabetes* 2016; **65**: 1255–1267.
77. Sen B, Guilluy C, Xie Z, Case N, Styner M, Thomas J *et al.* Mechanically induced focal adhesion assembly amplifies anti-adipogenic pathways in mesenchymal stem cells. *Stem Cells* 2011; **29**: 1829–1836.
78. Mathieu PS, Loboa EG. Cytoskeletal and focal adhesion influences on mesenchymal stem cell shape, mechanical properties, and differentiation down osteogenic, adipogenic, and chondrogenic pathways. *Tissue Eng - Part B Rev* 2012; **18**: 436–444.
79. Ruiz-Ojeda FJ, Wang J, Bäcker T, Krueger M, Zamani S, Rosowski S *et al.* Active integrins regulate white adipose tissue insulin sensitivity and brown fat thermogenesis. *Mol Metab* 2021; **45**: 101147.
80. Gao H, Guo Y, Yan Q, Yang W, Li R, Lin S *et al.* Lipoatrophy and metabolic disturbance in mice with adipose-specific deletion of kindlin-2. *JCI insight* 2019; **4**: e128405.
81. Lange M, Angelidou G, Ni Z, Criscuolo A, Schiller J, Blüher M *et al.* AdipoAtlas: A reference lipidome for human white adipose tissue. *Cell reports Med* 2021; **2**: 100407.
82. Collins JM, Neville MJ, Pinnick KE, Hodson L, Ruyter B, van Dijk TH *et al.* De novo lipogenesis in the differentiating human adipocyte can provide all fatty acids necessary for maturation. *J Lipid Res* 2011; **52**: 1683–1692.
83. Heemskerk MM, Giera M, Bouazzaoui F El, Lips MA, Pijl H, van Dijk KW *et al.* Increased PUFA Content and 5-Lipoxygenase Pathway Expression Are Associated with Subcutaneous Adipose Tissue Inflammation in Obese Women with Type 2 Diabetes. *Nutrients* 2015; **7**: 7676–7690.
84. Grzybek M, Palladini A, Alexaki VI, Surma MA, Simons K, Chavakis T *et al.* Comprehensive and quantitative analysis of white and brown adipose tissue by shotgun lipidomics. *Mol Metab* 2019; **22**: 12–20.
85. Dyall SC, Balas L, Bazan NG, Brenna JT, Chiang N, da Costa Souza F *et al.* Polyunsaturated fatty acids and fatty acid-derived lipid mediators: Recent advances in the understanding of their biosynthesis, structures, and functions. *Prog Lipid Res* 2022; **86**: 101165.
86. Gealekman O, Guseva N, Hartigan C, Apotheker S, Gorgoglione M, Gurav K *et al.* Depot-specific differences and insufficient subcutaneous adipose tissue angiogenesis in human obesity. *Circulation* 2011; **123**: 186–194.

87. Bays HE, González-Campoy JM, Bray GA, Kitabchi AE, Bergman DA, Schorr AB *et al.* Pathogenic potential of adipose tissue and metabolic consequences of adipocyte hypertrophy and increased visceral adiposity. *Expert Rev Cardiovasc Ther* 2008; **6**: 343–368.
88. Guilherme A, Virbasius J V., Puri V, Czech MP. Adipocyte dysfunctions linking obesity to insulin resistance and type 2 diabetes. *Nat Rev Mol Cell Biol 2008 95* 2008; **9**: 367–377.
89. Madamanchi NR, Vendrov A, Runge MS. Oxidative stress and vascular disease. *Arterioscler Thromb Vasc Biol* 2005; **25**: 29–38.
90. Lum H, Roebuck KA. Oxidant stress and endothelial cell dysfunction. *Am J Physiol Cell Physiol* 2001; **280**: C719-41.
91. Potente M, Carmeliet P. The Link Between Angiogenesis and Endothelial Metabolism. *Annu Rev Physiol* 2017; **79**: 43–66.
92. Li X, Sun X, Carmeliet P. Hallmarks of Endothelial Cell Metabolism in Health and Disease. *Cell Metab* 2019; **30**: 414–433.
93. Kalucka J, Bierhansl L, Conchinha NV, Missiaen R, Elia I, Brüning U *et al.* Quiescent Endothelial Cells Upregulate Fatty Acid β-Oxidation for Vasculoprotection via Redox Homeostasis. *Cell Metab* 2018; **28**: 881-894.e13.
94. Festa J, AlZaim I, Kalucka J. Adipose tissue endothelial cells: insights into their heterogeneity and functional diversity. *Curr Opin Genet Dev* 2023; **81**: 102055.
95. Chivite I, Monelli E, Munar-Gelabert M, Gómez-Valadés AG, Alvarado-Diaz A, Pozo M *et al.* Deletion of Mfn2 in endothelial cells triggers a mitohormetic response that improves systemic metabolism and healthspan in mice. *Cell Metab* 2026; **38**: 546-564.e11.

Figures

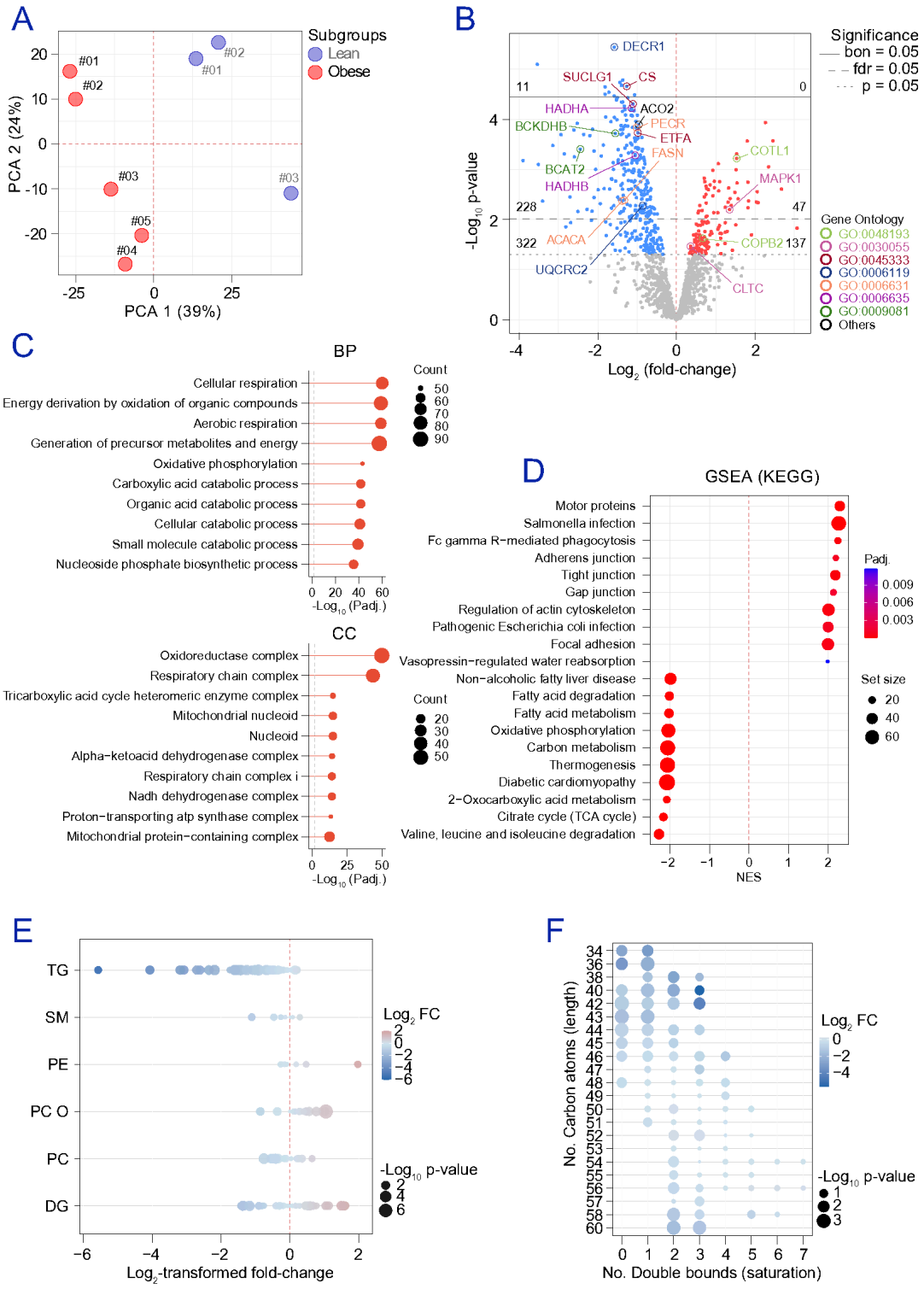


Figure 1

Obesity influences adipocyte protein and lipid-signatures. (a) PCA shows the clustering of adipose cells obtained in gallstone surgery patients with (BMI>30 kg/m^2) and without (BMI<25 kg/m^2) obesity. **(b)** The scatter dot plot shows DAPs up (red) and down-regulated (blue) in “obese” (n=5) vs “lean” (n=3) adipocytes. Statistical significance was assessed by employing two-tailed Bayesian moderated t-tests and assuming equal variance in unpaired comparisons. Dots in grey show proteins meeting our

exclusion criteria (nominal p-value≥0.05). Colored labels indicate protein landmarks of GO pathways significantly regulated after weight loss (WL), i.e., golgi-vesicle transport (GO:0048193), cell-substrate junction (GO:0030055), cellular respiration (GO:0045333), oxidative phosphorylation (GO:0006119), fatty acid metabolism (GO:0006631), fatty acid beta-oxidation (GO:0006635), and/or branched-chain amino acid metabolism (GO:0009081). **(c)** ORA in a GO computational framework. Additional details are provided in **Table S7**. **(d)** GSEA (KEGG) annotations revealed, among others, the downregulation of metabolic processes related to mitochondrial performance and lipid handling in subjects with obesity. **(e)** Lipidomes conducted in “obese” (n=8) vs “lean” (n=9) adipocytes show apparent variations on the abundance of triglycerides (TG), sphingomyelins (SM), phosphatidylethanolamines (PE), phosphatidylcholine-ethers (PC O) and phosphatidylcholines (PC), and diglycerides (DG). Other lipid families were dismissed due to the very low amounts detected. Bubble plot in **(f)** shows variations in TG species, segregated according to their saturation (nº double bounds) and length (nº carbon atoms). Differential abundance of lipids was considered significant based on an absolute $\log_2$ FC value≥0.58 and nominal p-value<0.05. Statistical significance was conducted by means of two-tailed Student’s t-tests. Source data for **Figures 2c** and **2d** is provided as a **Source data file**.

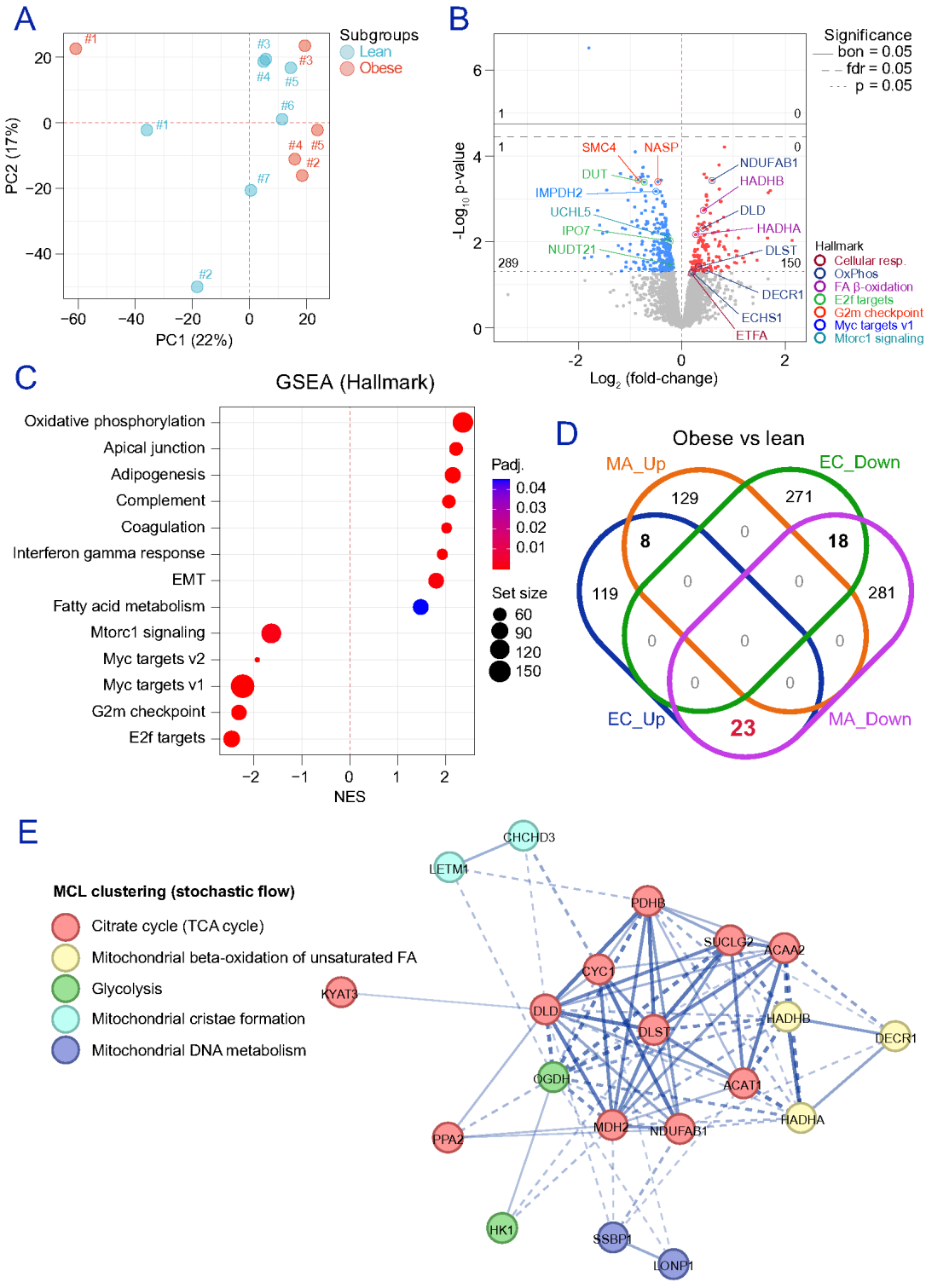


Figure 2

Mapping obesity-associated alterations in adipose-resident EC. (a) PCA shows the clustering of EC obtained in gallstone surgery patients with (BMI>30 kg/m^2) and without (BMI<25 kg/m^2) obesity. **(b)** The scatter dot plot shows DAPs up (red) and down-regulated (blue) in “obese” (n=5) vs “lean” (n=7) EC. Statistical significance was assessed by employing two-tailed Bayesian moderated t-tests and assuming equal variance in unpaired comparisons. Dots in grey show proteins meeting our exclusion criteria

(nominal p-value≥0.05). Colored labels point at protein landmarks of significance in relevant pathways. **(c)** GSEA (Hallmark) annotations revealed, among others, the downregulation of cell cycle-related pathways and the upregulation of OXPHOS, mitochondrial performance, and lipid handling in subjects with obesity. **(d)** Integration of protein datasets obtained in ex vivo isolated “obese” vs “lean” adipose-resident cells show an apparent number of proteins (23) with opposite sign in EC and mature adipocytes (MA). **(e)** Gene concept network depicting the relationships between these 23 proteins. The Markov Cluster Algorithm (MCL) was used to find natural clusters based on the stochastic flow (inflation parameter: 5). Pathways with the same color correspond to the same cluster. Line thickness indicates the strength of data support. Dotted lines show edges between clusters. Source data is provided as a **Source data file**.

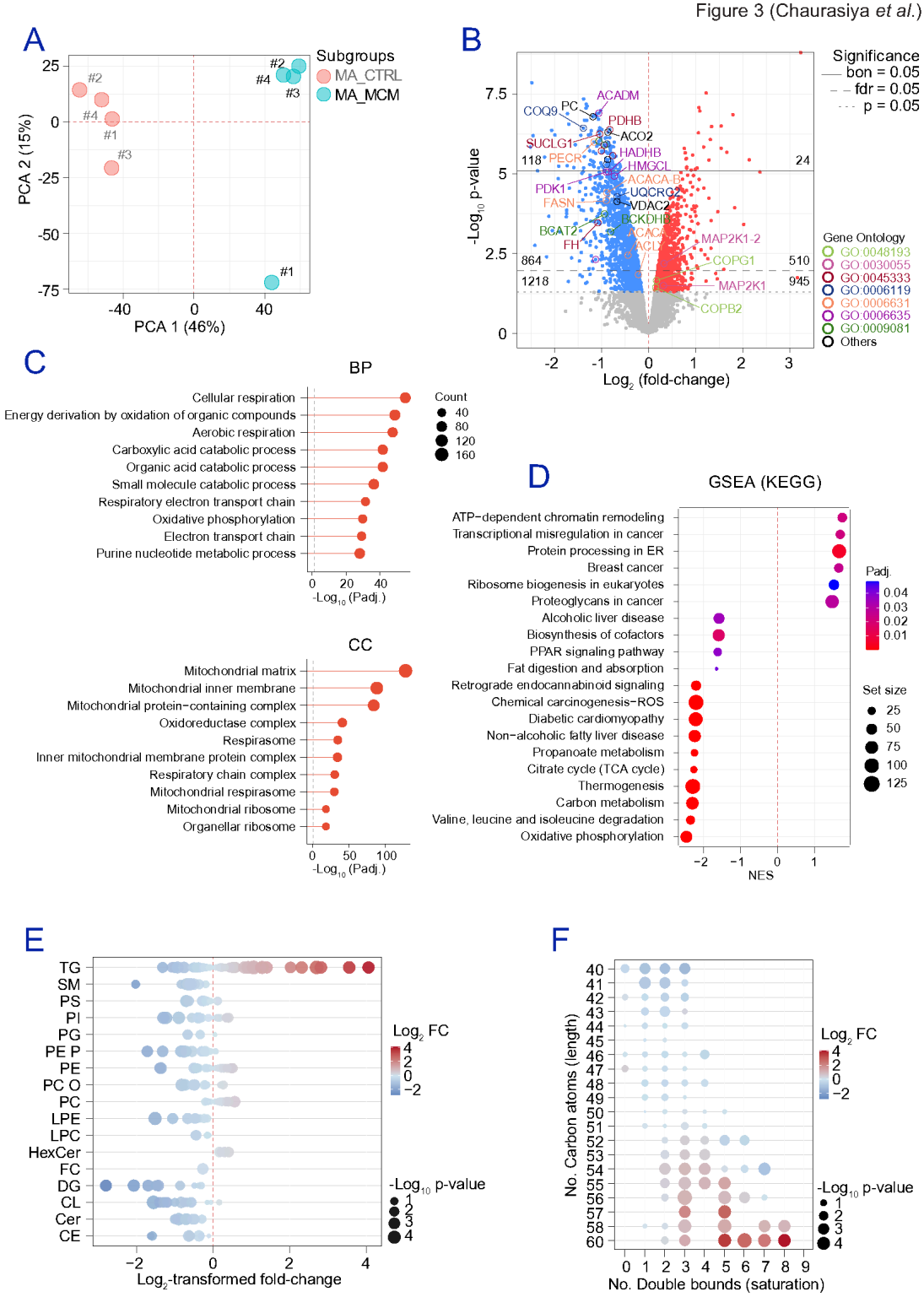


Figure 3

Macrophage-derived cytokines impact molecular patterns in adipocytes. (a) PCA shows the clustering of primary adipocyte cultures upon treatment with LPS-conditioned macrophage media (MCM) vs control (fresh macrophage media), n=4/group. **(b)** The volcano plot shows DAPs up (red) and down-regulated (blue) in MCM-activated adipocytes. Statistical significance was assessed by employing two-tailed Bayesian moderated t-tests and assuming equal variance in unpaired comparisons, and dots in

grey show proteins meeting our exclusion criteria (nominal p-value≥0.05). Colored labels point at protein landmarks of GO pathways significantly regulated in activated cells, as detailed in **Figure 1** legend. **(c)** ORA enrichment terms in a GO computational framework. Additional details are provided in **Table S9**. **(d)** GSEA (KEGG) annotations according to the main function of altered protein hubs. **(e)** Lipidomes conducted in control (n=3) and MCM-activated (n=3) adipose cells showed the modulation of many glycero- and sphingolipid species: TG, SM, phosphatidylserines (PS), phosphatidylinositols (PI), phosphatidylglycerols (PG), PE and PE based plasmalogens (PE P); PC and PC O; lysophosphatidylethanolamines (LPE), lysophosphatidylcholines (LPC), hexosylceramides (HexCer), FC, DG, cardiolipins (CL), ceramides (Cer), and cholesteryl esters (CE). The modulation of phosphatidic acids (PA) is not shown due to their very low amounts. Bubble plot in **(f)** shows TG species segregated according to the saturation (nº double bounds) and FA length (nº carbon atoms). Statistical significance was assessed by employing two-tailed Student's t-test between study and control group. Differential abundance of lipids was identified based on an absolute $\log_2$ FC value≥0.58 and p-value<0.05. Source data for **Figures 3c** and **3d** is provided as a **Source data file**.

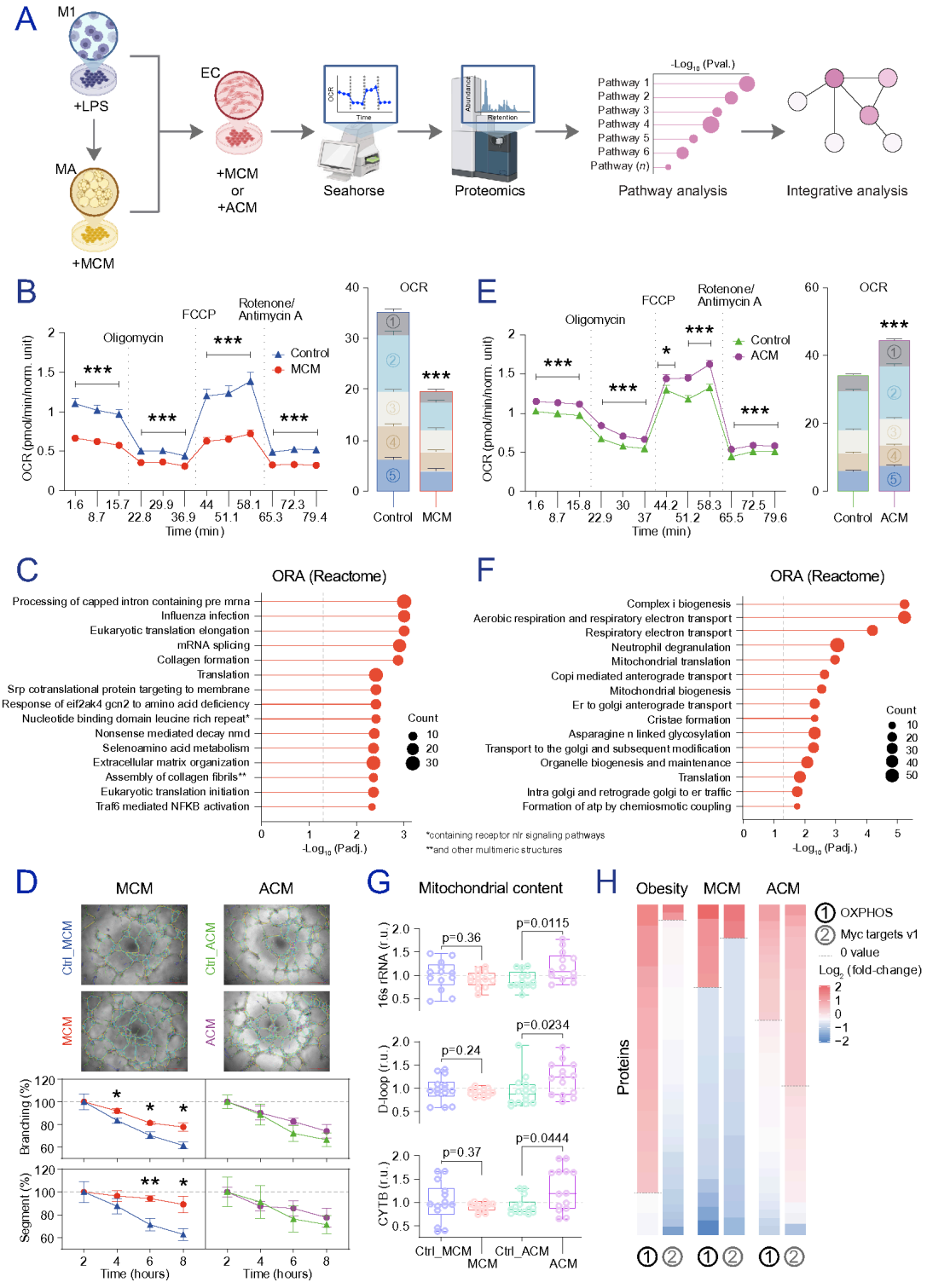


Figure 4

Macrophage and adipocyte-conditioned media reproduce different EC responses. (a) Schematic representation of our workflow in HAMEC cultures. **(b)** Seahorse mitochondrial stress flux analysis and measures of oxygen consumption rate (OCR) in HAMEC cultures treated with 1% MCM for 72 hours (3 assays). **(c)** ORA of proteomic results (see in **Figure S6a-g**) and pathway interpretation according to the open-source, curated and peer-reviewed Reactome database. **(d)**Comparative network patterns of

HAMEC and time-course network analysis according to the “Endothelial Tube Formation Assays” (ETFA). Phase contrast images with the superposition of vectorial objects were obtained from computer analysis using the customized “Angiogenesis Analyzer” for ImageJ. In the example provided (6 hours), in green, *Branches*; magenta, *Segments*; red surrounded by blue, *Junctions*; cyan, *Meshes*; violet, *Anchorage Junctions*; red circle, *Sphere*. ETFA scale bar, in red: 750 µm. **(e)** Seahorse mitochondrial stress flux analysis and OCR measures in HAMEC when treated with 10% ACM for 72 hours (3 assays). **(f)** ORA of proteomic results (see in **Figure S7a-g**), and pathway interpretation according to Reactome. **(g)** Analysis of mitochondrial components in MCM and ACM-activated HAMEC (3 assays). **(h)** The heatmap shows, in each dataset, the significant modulation of scoreboard proteins in OXPHOS and Myc targets-related biological processes (Hallmark). In Seahorse assays, (**1**) spare respiratory capacity, (**2**) maximal respiration, (**3**) basal respiration, (**4**) ATP-production coupled respiration, and (**5**) non-mitochondrial oxygen consumption. Mann-Whitney test (Holm-Šídák method for multiple comparisons). *p<0.05, **p<0.01, ***p<0.001. Source data is provided as a **Source data file**.

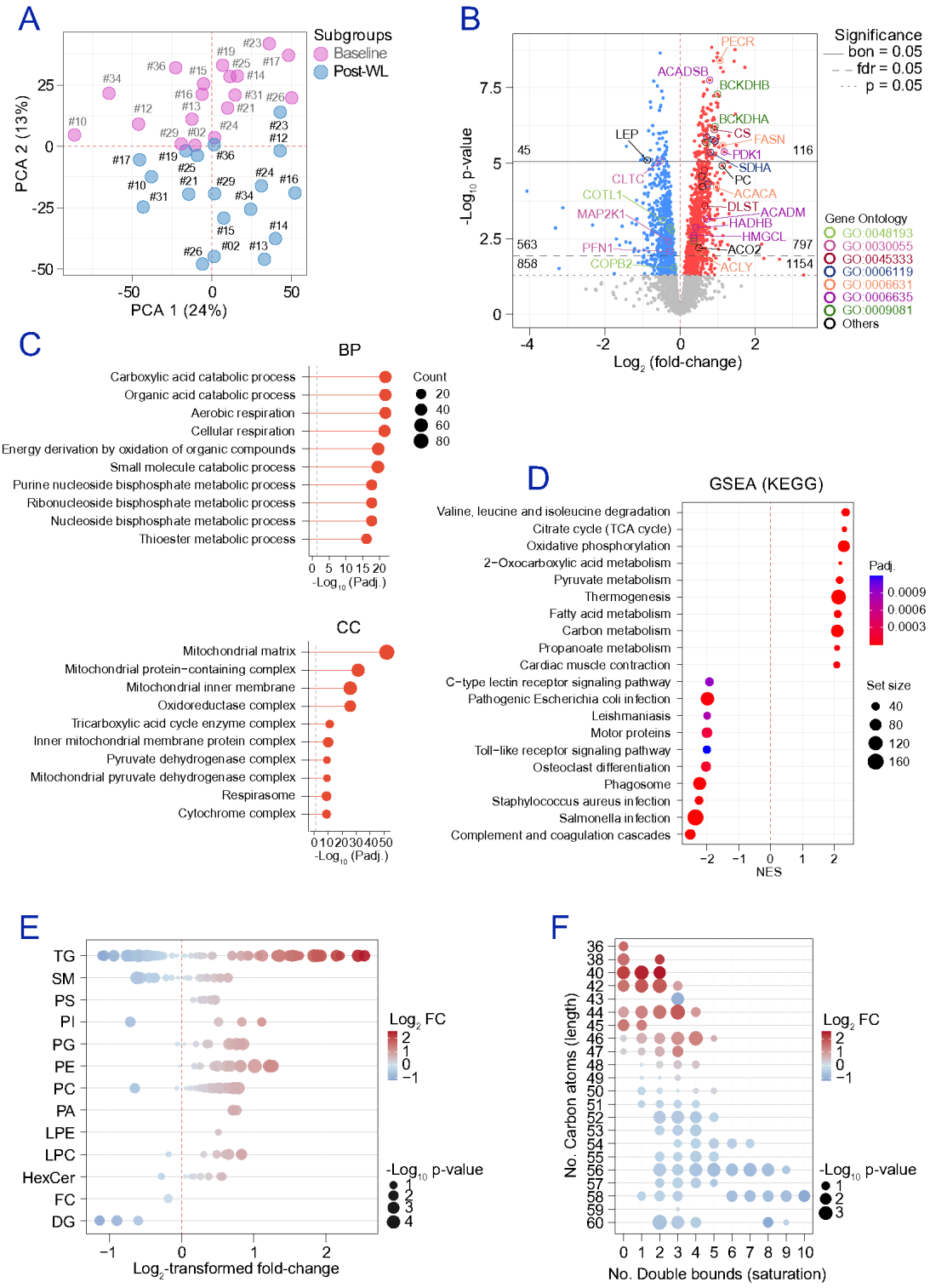


Figure 5

Weight loss reshapes adipose tissue protein and lipid landscapes. (a) PCA shows the clustering of fat samples obtained at baseline and following weight loss (WL) (n=18). **(b)** The volcano plot shows DAPs up (red) and down-regulated (blue) in subcutaneous adipose tissue after WL. Statistical significance was assessed by employing two-tailed Bayesian moderated t-tests, assuming equal variance in paired comparisons. Dots in grey show proteins meeting our exclusion criteria (nominal p-value≥0.05).

Coloured labels point at protein landmarks of GO pathways, as detailed in **Figure 1**. **(c)** Bubble plots created by applying ORA to enrichment terms in a GO computational framework. ORA pathways were segregated in Biological processes (BP) and Cellular components (CC). Additional details are provided in **Table S12**. **(d)** Gene set enrichment analysis (GSEA) and Kyoto encyclopaedia of genes and genomes (KEGG) annotations confirmed the upregulation of mitochondrial processes mostly related to fatty acid metabolism, running together with the downregulation of immune response determinants after WL. **(e)** The dynamic nature of lipids in bulk adipose tissue before-after WL (n=20) pointed at the modulation of a number of glycerophospholipid and sphingolipid species, including TG, SM, PS, PI, PG, PE, PC, PA, LPE and LPC; HexCer, FC, and DG. Bubble plot in **(f)** shows modulation of TG species, segregated according to the degree of saturation (nº double bounds) and length (nº carbon atoms) of fatty acids (FA). Lipid concentrations were normalized based on the total amount within each lipid class, followed by $\log_2$ transformation for conducting two-tailed Student's t-test between study and control groups. Differential abundance of lipids was identified based on an absolute $\log_2$ fold-change (FC) value≥0.58 and nominal p-value<0.05. Source data for **Figures 5c** and **5d** are provided as a **Source data file**.

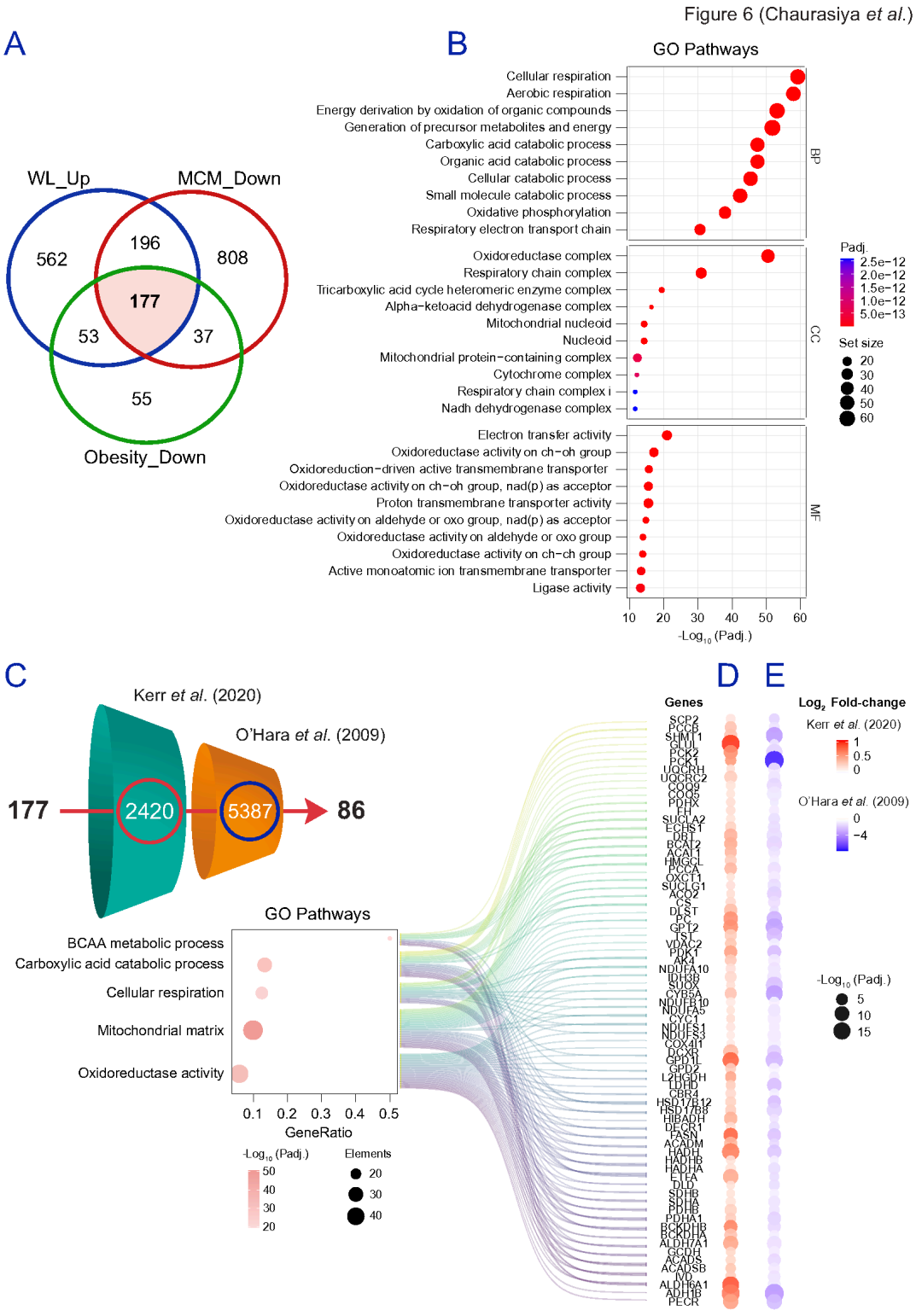


Figure 6

Restoration of fat metabolism after WL lies in adipocytes. (a) The Venn diagram shows the number of proteins that are upregulated in bulk adipose tissue after WL (blue circle), but decreased in adipocyte cultures when challenged with macrophage-derived cytokines (red circle), and in “obese” when compared to “lean” isolated adipocytes (green circle). For the selection we considered proteins showing unadjusted two-tailed p-values<0.05 in Bayesian moderated t-tests. Common elements are represented

by the intersections of circles. The intersection faintly inked shows 177 conjointly regulated proteins. The pathways underlined according to the ORA (GO) are provided in **(b)**. The funnel diagram in **(c)** depicts the comprehensive pipeline used to shortlist potential target proteins (genes) across independent transcriptional studies in bulk fat after surgery-induced WL [60] and experiments in MCM-inflamed SGBS-derived adipocytes [61] (see in **Figure S10a** for further detail on our experimental framework). Bubble plots in **(d)** and **(e)** shows how these gene candidates behave in those alternative datasets, and the pathways they belong to. Source data are provided as a **Source data file** (**Figures 6b**).

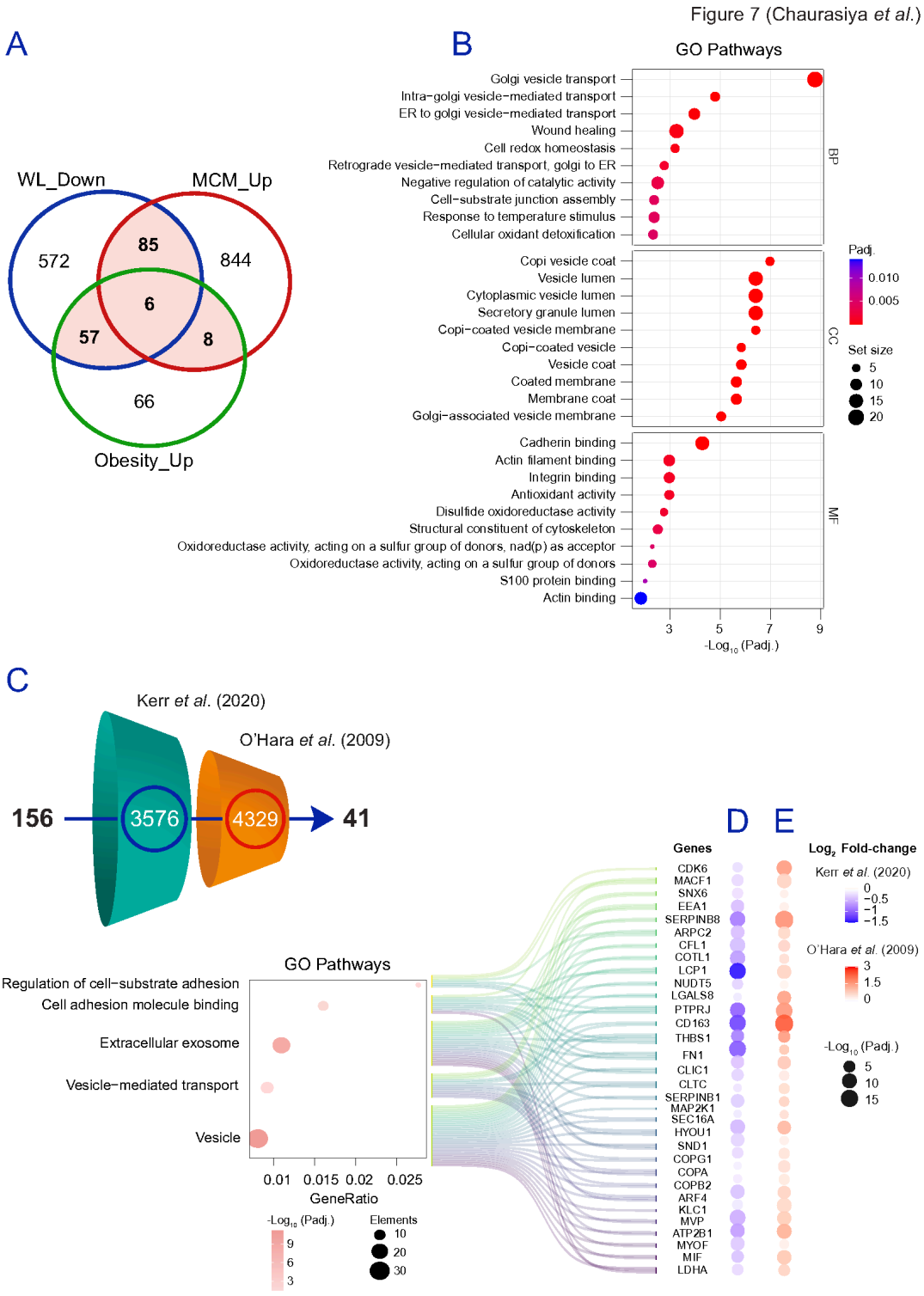


Figure 7

Increased adipocyte vesicle transport and ECM adherence in obesity. (a) The Venn diagram shows the number of proteins that are coincidentally downregulated in adipose tissue after WL (blue circle), but increased in inflamed adipocyte cultures (red circle), and “obese” adipocytes (green circle). For the selection we considered proteins with unadjusted two-tailed p-values<0.05 in Bayesian moderated t-tests. The colored intersections include a total of 156 proteins showing at least 2 over 3 matches, when

considering together our results in vivo, in vitro, and ex vivo. The pathways represented in this list of proteins are listed in **(b)**. The pipeline in **(c)** led us to cut down to 41 the gene (protein) candidates significantly associated, also at the transcriptional level, with **(d)** WL and **(e)** adipocyte inflammation. See in **Figure S10a** for further detail on our experimental workflow. Source data are provided as a **Source data file** (**Figure 7b**).

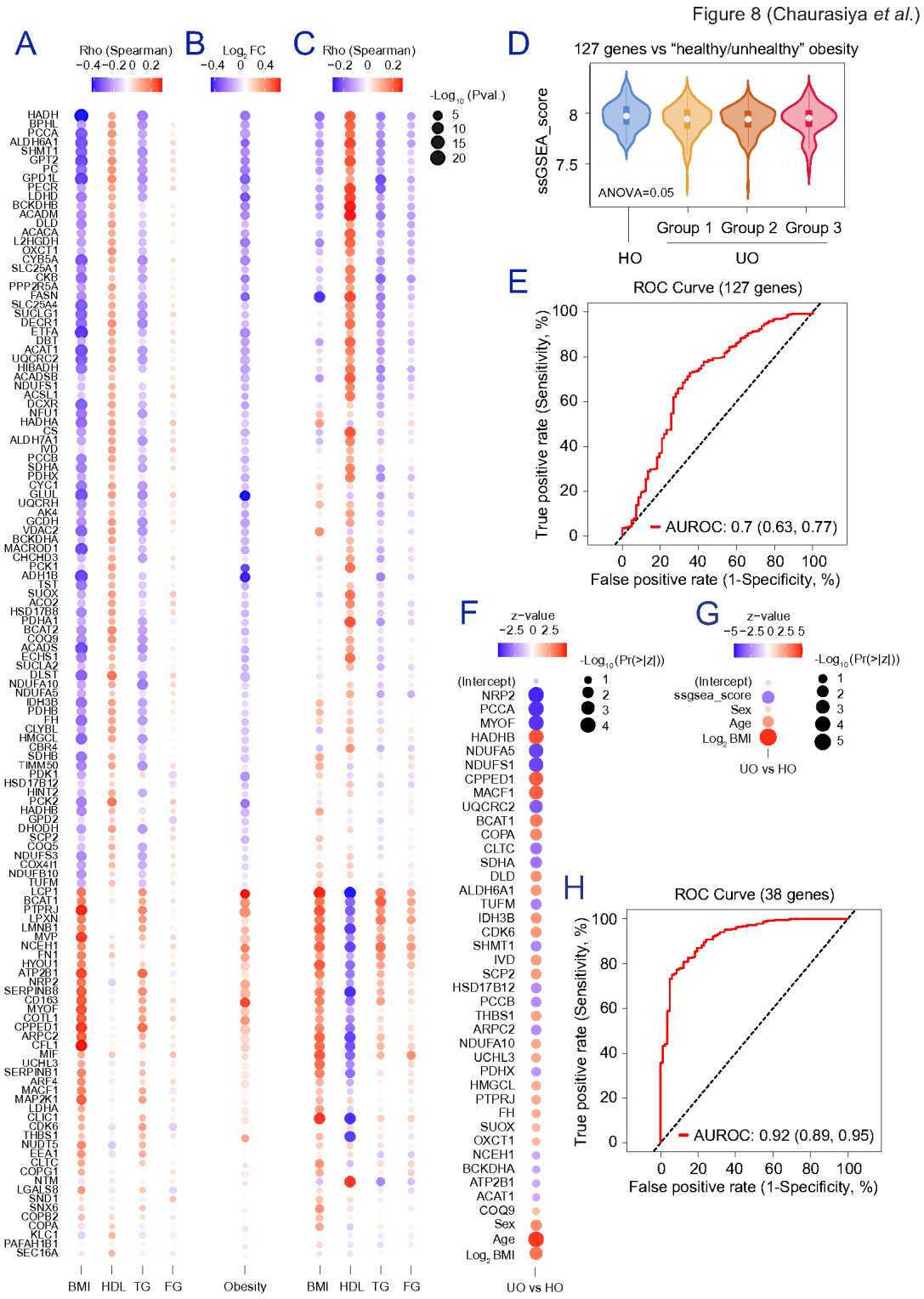


Figure 8

Gene association with obesity-related metabolic outcomes. Bubble plots in **(a)** (METSIM [27,28]) and **(c)** (ADIPOMIT [30]) show in cross-sectional studies Spearman's rank correlation coefficients (Rho) and two-tailed p-values for correlations between metabolic traits (i.e., BMI, HDL, TG, and fasting glucose) and the expression of our 127 gene candidates in adipose tissue. Bubble plot in **(b)** (Finnish Twin Cohort [29]) show the Log_2 fold-change (FC) and false discovery rate (FDR) p-values, when comparing the expression of these genes in the adipose tissue of monozygotic twin pairs with vs without obesity. **(d)** The violin plot and **(e)** ROC curve show the ability of this 127 gene cluster to segregate "healthy" (HO) and "unhealthy" (UO) obesity. Groups 1 to 3 indicate the number of metabolic comorbidities (i.e., dyslipidemia, hypertriglyceridemia, and/or hyperglycemia) observed, together with obesity, in ADIPOMIT participants. Bubble plots **(f)** and **(g)** show the stepwise regression model built upon our 127 gene candidates, along with sex, age and BMI as covariates, to stablish the final model of 38 genes, **(h)** able to better pick up the appearance of metabolic disturbances defining UO. See in **Figure S10b** for further details on our experimental workflow. Source data are provided as a **Source data file**.

Figure 9

Adipocyte and EC proteins defining obesity-related meta-inflammation. Venn diagrams show the number of proteins that are coincidentally **(a)** down or **(b)** up-regulated in MCM (blue circle) and ACM (red circle)-activated HAMEC, and in “obese” vs “lean” EC (green circle). For the selection we considered proteins with unadjusted p-values<0.05 in two-tailed Bayesian moderated t-tests. The coloured intersections highlight the number of proteins showing ≥2 over 3 potential matches, when considering

together our results in vitro, ex vivo, and in vivo. Funnel diagrams show the pipeline we followed to cut down the gene (protein) candidates associated, also at the transcriptional level, with WL in three independent bulk adipose tissue transcriptomes. Bubble plot in **(c)** shows Spearman's rank correlation coefficients (Rho) and two-tailed p-values for correlations between BMI, HDL, fasting TG, and blood glucose and the expression of our 34 gene candidates in the obese population of the ADIPOMIT study. See in **Figure S11a** for further detail on our experimental framework. Bubble plot in **(d)** shows the stepwise regression model built upon our proteomic-transcriptomic results, along with sex, age, and BMI as covariates, to stablish the final model of 46 genes, able to better pick up the appearance of metabolic disturbances defining UO, as shown in **(e)**. Next, bubble plot in **(f)** and ROC curve in **(g)** show the performance of our curated, final 46-gene signature in dissociating "healthy" (HO) from "unhealthy" (UO) obesity also in the KOBS cohort. Source data are provided as a **Source data file**.

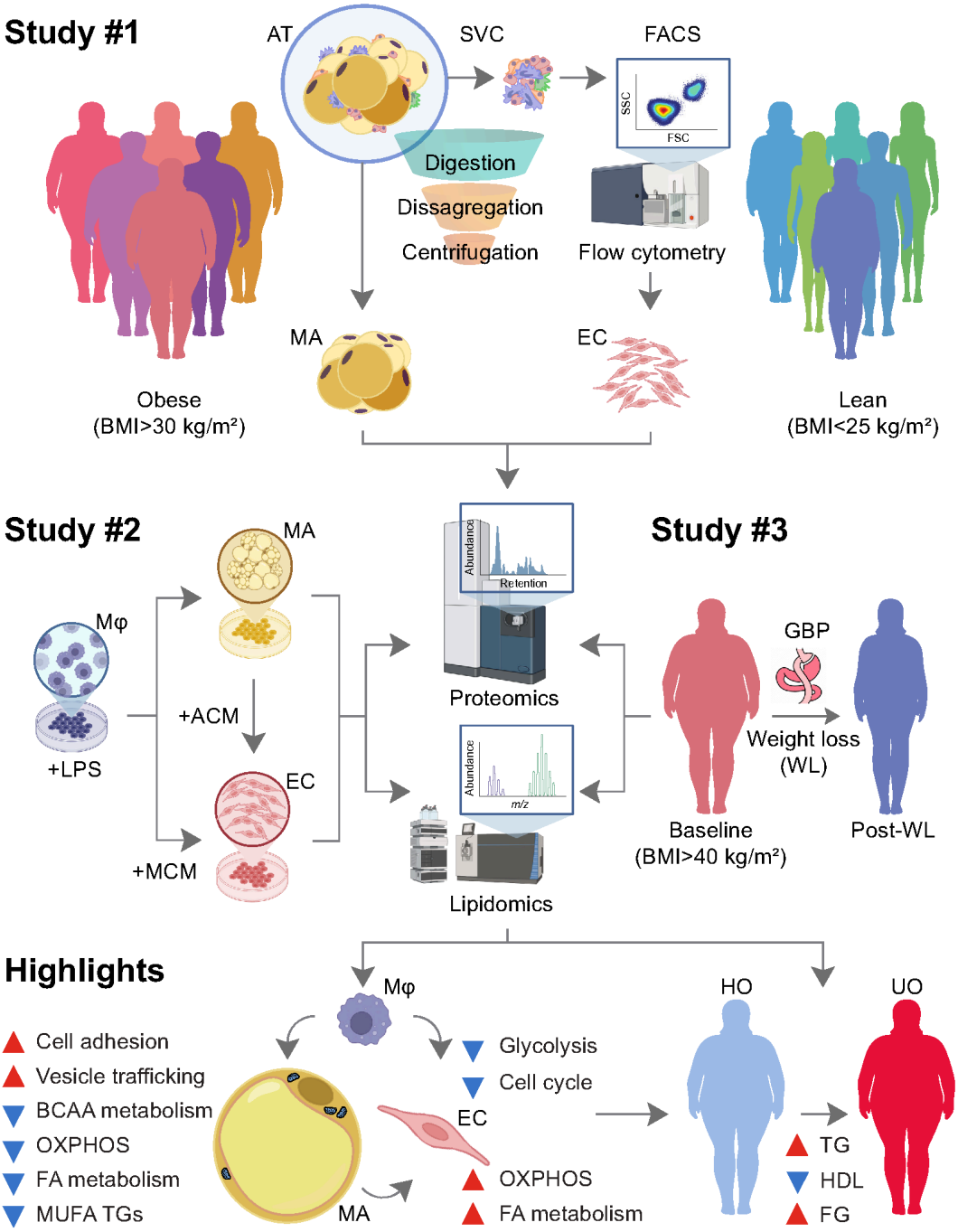


Figure 10

An adipose cell-type-informed, cross-context framework to identify molecular signatures of metabolic vulnerability in obesity. Here, we used a layered design to **(#1)** define, in human adipose tissue (AT), obesity-associated, cell-type-resolved molecular phenotypes in both mature adipocytes (MA) and endothelial cells (EC) within stromal vascular cells (SVC), **(#2)**mimic an obesity-like inflammatory milieu and probe adipocyte-to-endothelial signaling using macrophage (MCM) and adipocyte-conditioned

media (ACM), and **(#3)**determine which obesity-associated features show evidence of recovery after surgery-induced weight loss (GBP) in bulk fat. We then curated a robust gene signature by intersecting obesity and inflammation-associated candidates with multiple transcriptomic datasets, and evaluated physiological relevance across human cohorts, including derivation of a refined gene signature capable of dissociating “healthy” (HO) from “unhealthy” (UO) obesity. Thereby, our study provides a comprehensive resource model for adipose cell-specific determinants acting as predictors of metabolic vulnerability in people living with obesity.

Supplementary Files

This is a list of supplementary files associated with this preprint. Click to download.

- ChaurasiyaetalSupplementalDataEEM.docx
- ChaurasiyaetalSuppFiguresEEM.pdf
- ChaurasiyaetalSupplementalDataEEM.xlsx
- ChaurasiyaetalSupplementalDataEEMRev1.docx